geosciences

MDPI

Article

Energy-Based Criterion of Thermal Stability of Ice-Rich Permafrost: A Case Study of the Ice Complex of Central Yakutia

Aleksandr Zhirkov [1,*], Mikhail Zheleznyak [1], Zhi Wen [2], Alexander Fedorov [1,3], Tonghua Wu [2], Pavel Konstantinov [1], Guoyu Li [2] and Vasylii Lytkin [1]

[1] Melnikov Permafrost Institute, Siberian Branch of the Russian Academy of Sciences, Yakutsk 677010, Russia; femnzhel@mpi.ysn.ru (M.Z.); anfedorov@mpi.ysn.ru (A.F.); pykonstantin@mpi.ysn.ru (P.K.); lytkinvm@mpi.ysn.ru (V.L.)

[2] State Key Laboratory of Cryospheric Science and Frozen Soil Engineering, Northwest Institute of Eco-Environment and Resources, Chinese Academy of Sciences, Lanzhou 730000, China; wenzhi@lzb.ac.cn (Z.W.); thuawu@lzb.ac.cn (T.W.); guoyuli@lzb.ac.cn (G.L.)

[3] Institute of Geography of the Russian Academy of Sciences, Moscow 119017, Russia

* Correspondence: zhirkov_af@mail.ru

Abstract

Thaw of ice-rich permafrost driven by climate warming and surface disturbance is a major geohazard for northern infrastructure, yet temperature-based monitoring indicators lose sensitivity as ground temperature approaches 0 °C. We propose an energy-based criterion of thermal stability built on the cold reserve, i.e., the enthalpy deficit of frozen ground relative to the onset of thawing, computed from standard site-investigation data with account for unfrozen water and ice wedges. An energy stability index, equal to the ratio of the cold reserve to the total heat input over a 30-year normative period, and the exhaustion time of the cold reserve are introduced. The heat load is derived from repeated borehole temperature logs. For the Ice Complex of Central Yakutia, the cold reserve of the 2–20 m layer is 2.6–4.1 GJ/m^2. Verification against 14 monitoring boreholes with 4 to 31 years between logging cycles yields heat loads of −0.7 to 2.2 MJ/(m^2·yr) and indices of 38–205 for natural landscapes, versus 5.1–13.0 MJ/(m^2·yr) and indices of 11.7 to 1.4 for disturbed thermokarst-affected sites, including a railway right-of-way. Surface wetting is the controlling factor. The criterion supports site ranking, prioritization of monitoring and mitigation, and rapid assessment of degradation time.

Keywords: cold reserve; thermal stability; ice-rich permafrost; Ice Complex; thermokarst; geohazards; climate change; borehole monitoring; infrastructure; Central Yakutia

Academic Editor: Hongyuan Liu

Received: 17 October 2026
Revised: 18 November 2026
Accepted: 20 November 2026
Published: 23 November 2026

Copyright: © 2026 by the authors. Licensee MDPI, Basel, Switzerland. This article is an open access article distributed under the terms and conditions of the Creative Commons Attribution (CC BY) license.

1. Introduction

Thaw of ice-rich permafrost is one of the most consequential geohazards of the cryosphere under a warming climate. Thermokarst, thaw settlement and loss of bearing capacity of frozen foundations threaten residential, transport and industrial infrastructure. About 70% of the current infrastructure in the Northern Hemisphere permafrost domain is located in areas with a high potential for thaw of near-surface permafrost by mid-century. One-third of pan-Arctic infrastructure lies in regions where thaw-related ground instability can cause severe damage [1]. Observed damage is already

substantial. Mitigation techniques such as convection embankments, thermosyphons and pile foundations have proven effective, but their efficient deployment requires a better understanding of where the risk is high [2]. By mid-century, 29–44% of roads and 23–34% of railways in the Arctic states are projected to be affected by permafrost degradation, with damage costs of 182–276 billion USD depending on the emission scenario, of which Russia bears the largest share [3]. For the Russian permafrost regions, about 54% of residential buildings, 20% of commercial and industrial structures and 19% of critical infrastructure are projected to be affected by permafrost degradation by the middle of the 21st century, and the Republic of Sakha (Yakutia), where 85% of the buildings stand on permafrost, is among the regions with the largest expected damage, about 21 billion USD [4]. In Central Yakutia, where the mean annual air temperature at Yakutsk rose from −9.6 °C in 1980 to −6.7 °C in 2019, thaw subsidence already damages houses, roads and power lines, and thermokarst lakes remain the main source of water for rural settlements [5]. The traditional land use of the rural Sakha population, hay-making and cattle and horse husbandry on the meadows of river terraces and alas depressions, depends on the state of permafrost [6], and the inhabitants of the region already perceive permafrost thaw as a risk to their livelihoods and culture [7,8]. Adaptation planning therefore needs quantitative, site-specific indicators of how large a thermal safety margin the frozen ground retains and how fast this margin is being consumed.

Present-day climate warming manifests itself most strongly in the permafrost zone, primarily where ice-rich deposits occur. In Central Yakutia, the Ice Complex deposits (loess-like loams and sandy loams with thick syngenetic ice wedges) occupy about 60% of the territory. Rising air temperature combined with surface disturbance has already increased the active-layer thickness on developed inter-alas landscapes by a factor of 1.4–2.7. The top of ice-rich horizons has been lowered at 0.03–0.16 m/yr, and thermokarst has been activated [9]. Numerical experiments for the ice-rich lowlands of northeast Siberia show that thermokarst-inducing processes, which most large-scale permafrost models neglect, substantially accelerate degradation under a warming climate [10], and a synthesis of observations across the Northern Hemisphere gives thaw subsidence rates of up to 2 cm/yr in ice-poor and more than 3 cm/yr in ice-rich permafrost, with higher rates in disturbed areas [11]. Surface subsidence rates range from 0.026–0.054 m/yr on inter-alas uplands to 0.17–0.24 m/yr near young thermokarst lakes [12].

The basic monitoring indicators, the mean annual ground temperature and the active-layer thickness [13], lose sensitivity as the temperature of ice-rich ground approaches 0 °C. An increasing share of heat is then spent on phase transitions at almost constant temperature, and degradation proceeds latently [14]. Model estimates show that about 44% of the heat absorbed by the permafrost-zone ground of the Northern Hemisphere in 1980–2018 was spent on melting ground ice [15]. This has stimulated the search for additional indicators: a geothermal stability criterion for the layer of annual heat turnover [16], climatic indices [17], temperature-trend [18,19] and probabilistic [20] criteria. Regional stability assessments are traditionally performed as ordinal scales and zoning maps based on ground temperature and ice content [21–23]. In the geoecological approach, the stability of cryogenic landscapes to technogenic disturbance is assessed using expert point scales with mapping of the hazard of cryogenic-process activation [24,25]. The result of such assessments is expressed in points and is linked neither to the magnitude of the thermal impact nor to the time over which the frozen state persists. Practice, including the development of regulations on permafrost protection, requires metric indicators. The energy (enthalpy) approach, rooted in the theory of annual heat turnovers [26,27] and in thermodynamic models of frozen ground [28], has not previously been developed into an applied stability criterion.

The aim of this study is to substantiate an applied energy-based criterion of the thermal stability of ice-rich permafrost based on the enthalpy characteristic of the frozen stratum and to parameterize it for the Ice Complex of Central Yakutia. A dimensionless energy stability index and a characteristic exhaustion time of the cold reserve are introduced. The enthalpy-based estimate of the heat flux from repeated temperature logging was previously used as a diagnostic quantity [29]. Here it is used for the first time as the normalizing quantity of a stability criterion. The criterion is verified against repeated temperature logs of fourteen boreholes of the monitoring network of the Melnikov Permafrost Institute, Siberian Branch of the Russian Academy of Sciences (MPI SB RAS). Eight boreholes are located at the Mundulakh, Amga, Yukechi, Yunkyur and Churapcha sites, and six on three cross-sections of the Tommot–Nizhny Bestyakh section of the Amur–Yakutsk Mainline railway (hereafter, the AYaM railway), each pairing a natural forest with the railway right-of-way. The location of the sites is described in Section 2.1. In terms of geohazard mitigation and adaptation, the criterion is intended to rank sites by the remaining thermal safety margin and to estimate the time horizon of thaw-related hazards relative to the service life of structures. The concept of the criterion is shown in Figure 1.

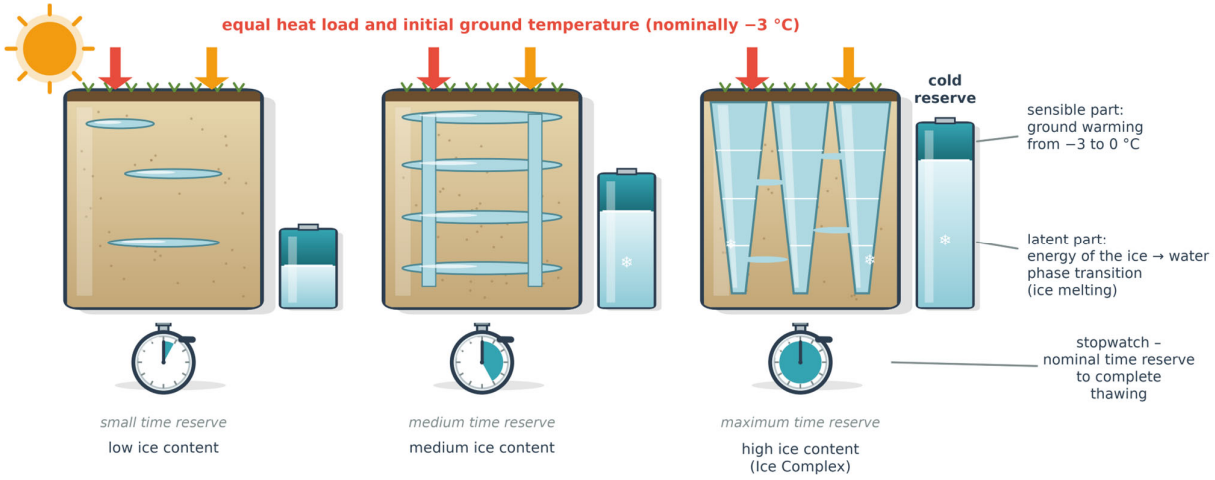

Figure 1. Concept of the energy-based criterion of thermal stability of ice-rich permafrost. Three ground blocks of equal size at the same initial temperature (nominally −3 °C) differ in ice content: low, medium and high (Ice Complex). The bar to the right of each block shows the cold reserve: the sensible part (teal) is the energy needed to warm the ground from the initial temperature to 0 °C, and the latent part (light blue) is the energy of the ice → water phase transition; with increasing ice content, the latent part and the total reserve increase many times. The stopwatches show the nominal time reserve until complete thawing under the same heat load: it is the smallest for the ice-poor ground and the largest for the Ice Complex. The red and orange arrows above each block depict the heat load on the ground surface, which is the same for the three blocks.

2. Materials and Methods

2.1. Study Area

The study area is located in Central Yakutia, in the middle reaches of the Lena River, on the Lena–Amga interfluve and the adjacent terraces of the Lena valley (Figure 2). The region is a low plain formed by the Bestyakh, Tyungyulyu, Abalakh and Magan erosion-accumulation terraces of the Lena and its tributaries [5].

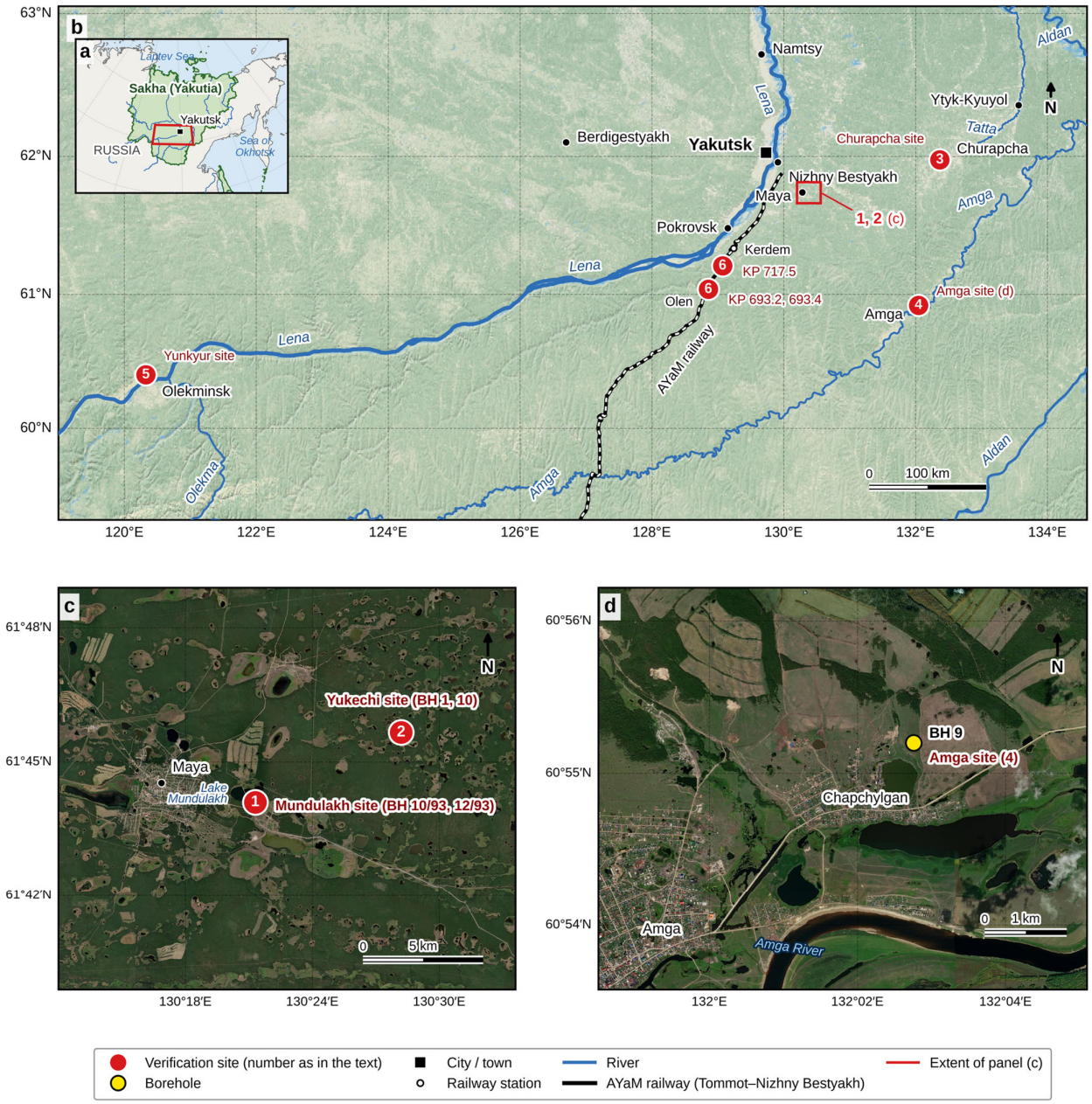

Figure 2. Location of the study sites and verification boreholes in Central Yakutia: (**a**) position of the study area (red rectangle) within the Sakha (Yakutia) Republic; (**b**) regional map; (**c**) the Mundulakh (1) and Yukechi (2) sites near the village of Maya; (**d**) the Amga site (4) near the village of Chapchylgan. Sites: 1—Mundulakh (boreholes 10/93 and 12/93); 2—Yukechi (boreholes 1 and 10); 3—Churapcha (boreholes 3 and 5); 4—Amga (borehole 9); 5—Yunkyur (borehole 2); 6—AYaM railway cross-sections KP 693.2, 693.4 and 717.5 (boreholes B-11, B-12, B-15, B-17, B-38/09 and B-39/09).

The climate is extremely continental. The mean annual air temperature at Yakutsk was −10.0 °C in 1961–1990 and −8.0 °C in 1981–2020 [30]. It rose from −9.6 °C in 1980 to −6.7 °C in 2019, i.e., by about 0.07 °C/yr, with mean monthly temperatures of about −38 °C in January and +20 °C in July [5]. Three climatic periods are distinguished in the instrumental record of Central Yakutia, 1930–1987, 1988–2006 and 2007–2018, with mean annual air temperatures of −10.3, −8.6 and −7.4 °C, and the active-layer depth under forest

increased by about 0.8 m over 1990–2018 [31]. Annual precipitation at Yakutsk is 230–240 mm [5,30]. The cold season lasts 210–215 days, and the snow cover reaches only 25–40 cm at the end of winter with a density of 170–200 kg/m^3 [30]. The thin snow cover and the long cold season maintain negative ground temperatures despite the warm summers.

The region lies in the continuous permafrost zone [32], and the permafrost thickness is 200–300 m [5]. Under larch forests of the middle taiga, the mean annual ground temperature is −1 to −3 °C and the active-layer thickness is 1.2–1.7 m [32]. On the inter-alas uplands, the mean annual temperature at the depth of zero annual amplitude ranges from −1.5 to −3 °C [33]. Under undisturbed forest, the temperature at this depth varies from −1.1 to −5.1 °C with an active layer of 1.2–2.0 m, whereas at cleared sites the active layer deepens to 1.5–2.8 m and the temperature rises to −0.5 to −4.1 °C [34]. The Ice Complex, loess-like silty loams and sandy loams with syngenetic ice wedges, forms the upper 12–25 m of the terraces. The wedge tops lie at a depth of 1.5–3.0 m, and the wedges are 2–3 m wide with a polygon spacing of 11–14 m [35,36]. The volumetric ice content of the inter-alas deposits, including wedge ice, is 0.4–0.6 and locally up to 0.8 [32]. The deposits are of continental origin and are regarded as non-saline (Section 4.2).

The zonal vegetation is middle taiga: larch forests with low shrubs and mosses on the loamy inter-alas uplands and pine forests on sandy terraces [32]. The landscape pattern is dominated by thermokarst. About 16,000 alas depressions with grassland meadows and lakes occupy about 17% of the Central Yakutian lowland [5], and the inter-alas uplands between them carry the undisturbed Ice Complex. Forest clearing, fires, ponding and construction trigger thermokarst, which passes through the stages of initial subsidence, a young depression and a drained alas [9,12,36].

The verification boreholes are located at six sites (Figure 2). The Mundulakh site (boreholes 10/93 and 12/93) lies on the inter-alas upland of the Lena–Amga interfluve east of Yakutsk, along the Nizhny Bestyakh–Mundulakh water pipeline, in a larch forest and in a young thermokarst depression on the pipeline right-of-way [30]. The Yukechi site (boreholes 1 and 10) is located on the Abalakh terrace 10 km east-north-east of the village of Maya, about 50 km south-east of Yakutsk, where thermokarst has been monitored since 1992 [12,37]. The Amga site (borehole 9) is located on the left bank of the Amga River near the village of Chapchylgan, about 4 km northeast of the village of Amga, on the surface of the Abalakh-level terrace, in a forb meadow with pronounced thermokarst relief and actively developing bylars (hummock-and-hollow microrelief of the initial stage) and without a lake. The borehole is the background (without restoration measures) site of the land-rehabilitation experiment of MPI SB RAS on disturbed arable land [38]. The terrace is composed of loams and sandy loams of the Ice Complex with large ice wedges [38]. The Churapcha site (boreholes 3 and 5) is located 4 km south-west of the village of Churapcha on the Lena–Amga interfluve, on the natural surface on both sides of the embankment of the R-504 Kolyma federal road, in an ice-rich meadow (borehole 3) and in a forest (borehole 5), both with hummock-and-hollow microrelief. The Yunkyur site (borehole 2) is located 5–7 km north-west of the town of Olekminsk in the Lena valley, at the south-western margin of the region, in a mixed spruce–birch forest undisturbed by human activity [39]. The section there consists of ice-rich loams and sandy loams with ice wedges at 4.9–7.2 m and is analogous to the Ice Complex of the inter-alas uplands. The AYaM railway cross-sections (KP 693.2, 693.4 and 717.5) are located 80–130 km south of Yakutsk on the Tommot–Nizhny Bestyakh section, where the right-of-way crosses larch forests on ice-rich silty loams in which the tops of ice wedges and massive ground ice lie at depths of 1.2–3.5 m [34,40]. The lithology and cryostructure of the deposits at the boreholes are summarized in Section 2.4.

2.2. Cold Reserve of Frozen Ground and Governing Relations

The thermal state of a frozen stratum is characterized by the amount of heat required to warm the ground of the design layer of unit area to the temperature at which phase transitions begin and to melt the ice it contains, i.e., by the enthalpy deficit relative to the thawed state. Hereafter, this quantity is called the cold reserve of permafrost. For a unit volume of ground at a temperature T below the temperature of the onset of thawing T_{bf} ($T_{bf} \approx 0$ °C for non-saline ground), the sensible component equals $C_f \cdot |T|$, and the latent component is determined by the heat of fusion of pore ice of mass $\rho_d \cdot [w_{tot} - w_w(T)]$, assuming no moisture migration and no change in dry density. Their sum gives the specific volumetric cold reserve at depth z, J/m³:

$$q_v(z) = C_f(z) \cdot |T(z)| + L_0 \cdot \rho_d(z) \cdot [w_{tot}(z) - w_w(T)] \quad (1)$$

where C_f is the volumetric heat capacity of frozen ground, J/(m³·°C); $T(z)$ is the mean annual ground temperature at depth z, °C; z is depth, m; $L_0 = 3.35 \cdot 10^5$ J/kg is the specific latent heat of the water–ice phase transition; ρ_d is the dry density of the ground, kg/m³; w_{tot} is the total water content (fraction, by mass of dry ground); and $w_w(T)$ is the unfrozen water content (fraction). Equation (1) is the standard calorimetric expression for the change in enthalpy of frozen ground [14,26]. Its latent component is equivalent to the normative expression of the Russian design code [41] (Equation (B.15)), and the dependence $w_w(T)$ is taken from laboratory data or from the normative procedure. Note that w_{tot} refers to the mass of dry ground: substituting the volumetric ice content defined in [42] for the difference $(w_{tot} - w_w)$ distorts the latent component by a factor of ρ_d/ρ_i, where $\rho_i = 917$ kg/m³ is the density of ice (a systematic error of up to 20–40%).

Ice Complex deposits require separate accounting for syngenetic ice wedges, whose volume is not reflected in the water content of the host sediments. Denoting by $a(z)$ the volumetric fraction of wedge ice, the volume-averaging rule gives

$$q_v^*(z) = [1 - a(z)] \cdot q_v(z) + a(z) \cdot \rho_i \cdot [c_i \cdot |T(z)| + L_0] \quad (2)$$

where q_v^* is the specific volumetric cold reserve including wedge ice, J/m³, and $c_i \approx 2.12 \cdot 10^3$ J/(kg·°C) is the specific heat capacity of ice [41] (Equation (B.9)). The value of $a(z)$ is estimated from the geometry of the polygonal network, from exposures and boreholes, or from geophysical data. For the Ice Complex of Central Yakutia, the ice content of the host sediments is 10–40%, reaching 50–80% when ice wedges are included [9]. The cold reserve of the design layer $[z_1, z_2]$ is

$$Q_S = \int q_v^*(z) \cdot dz, \quad z \in [z_1, z_2] \quad (3)$$

The quantity Q_S is expressed in J/m² and, by construction, is analogous to computing heat turnovers through the change in heat content of the stratum [26,27]. The upper boundary z_1 should preferably coincide with the permafrost table, and the lower boundary z_2 should be set at the base of the ice-rich horizon or of the layer of annual heat turnover [43]. When sites are compared, z_2 is assigned uniformly.

For ice-rich ground at $|T| = 1.5$–3 °C, the sensible component does not exceed 2–5%. For ice-poor cold sands, however, its share reaches 15–20% or more, so in the general case both components are taken into account. For fine-grained and saline ground with intense phase transitions over the range of negative temperatures, an equivalent formulation uses the effective heat capacity $C_{ef} = C_f + L_0 \cdot \rho_d \cdot (\partial w_w / \partial T)$, J/(m³·°C), with the actual temperature of the onset of thawing: for a state function both forms are identical, the protracted shape of the unfrozen-water curve is accounted for exactly in (1), and the difference matters only in the transient heat-conduction problem [28].

2.3. Energy Stability Index and Exhaustion Time of the Cold Reserve

The cold reserve is a capacity characteristic: it shows how much heat the ground can absorb before the design layer thaws completely, but it does not determine the rate of degradation. Stability is governed by the ratio of the capacity to the external load, taken here as the long-term mean net heat flux density into the frozen stratum q_r, MJ/(m²·yr), equal to the difference between the heat turnovers of the warm and cold periods of the year at the permafrost table [26,27]: in a quasi-stationary climate $q_r \approx 0$, whereas under warming or surface disturbance $q_r > 0$. The main way to determine q_r is enthalpy processing of repeated borehole temperature logs: the cold reserves are computed by (1)–(3) from the temperature profiles at times t_1 and t_2 (years), and their difference is divided by the time interval:

$$q_r = \frac{Q_S(t_1) - Q_S(t_2)}{t_2 - t_1} \quad (4)$$

Equation (4) follows from the heat balance of the design layer and contains no empirical coefficients. When the permafrost table moves downward, a boundary term is added (Equation (7)). A similar estimate from repeated temperature profiles gave 0.13–0.39 W/m², i.e., about 4–12 MJ/(m²·yr), for natural landscapes of interior Alaska [29]. A scenario-based specification of the expected thaw rate v, m/yr, is also possible, with conversion $q_r = v \cdot q_v^*$. We define the energy stability index as the ratio of the cold reserve to the total heat input over a normative period τ_0:

$$I_E = \frac{Q_S}{q_r \cdot \tau_0} \quad (5)$$

The period τ_0 is taken equal to 30 years for three reasons. First, 30 years is the standard averaging period of climatological normals adopted by the World Meteorological Organization. It is long enough to smooth interannual variability and short enough to follow the changing climate [44]. The load q_r is thus averaged over the same time scale as the climatic forcing that produces it. Second, 30 years corresponds to the penetration of the climatic signal into the design layer. For the thermal diffusivity of frozen ice-rich loams, $\kappa = (0.9–1.3)\cdot10^{-6}$ m²/s, the e-folding depth of a temperature wave with a period of 30 years, $d = (\kappa\tau_0/\pi)^{1/2}$, is 16–20 m, which is close to the lower boundary of the design layer, $z_2 = 20$ m. A shorter period would characterize only the upper part of the layer, and a longer one would add little information about the design layer. Third, 30 years is comparable to the design service life of linear and industrial structures on permafrost and to the mid-century horizon of infrastructure risk assessments [1,4]. The choice of τ_0 affects only the scaling of I_E and the class boundaries. The exhaustion time t_Q (Equation (6)) does not depend on τ_0, and the ranking of sites by I_E is the same for any τ_0. The index is related to the characteristic exhaustion time of the cold reserve t_Q, years:

$$t_Q = \frac{Q_S}{q_r} \quad (6)$$

Equations (2), (5) and (6) are introduced in this study. Based on the index value, four stability classes are proposed: stable ($I_E \geq 10$), conditionally stable ($3 \leq I_E < 10$), weakly stable ($1 \leq I_E < 3$) and unstable ($I_E < 1$), in which case the cold reserve is exhausted within the normative period. The thresholds are justified in Section 3.1. They may be refined as the sample grows.

The linear extrapolation (6) is conservative: under unchanged surface conditions, the deepening of the thaw front is accompanied by a decrease in the heat flux reaching the front, so the actual time is longer than t_Q. An upper estimate is given by the Stefan approximation [26] $t_{St} = q_v^* \cdot H^2/(2\lambda_t \cdot T_s)$, where λ_t is the thermal conductivity of the thawed zone, W/(m·°C); T_s is the mean surface temperature over the degradation period, °C; and

H is the layer thickness, m. In practical assessments, it is advisable to report the interval [t_Q; t_{SI}]. The criterion is a rapid assessment tool and does not replace numerical modeling. However, it is computed directly from site-investigation and monitoring data.

2.4. Input Data

The parameterization characterizes a typical inter-alas section of the Ice Complex described in Section 2.1 rather than a specific site. The section scheme is shown in Figure 3. The adopted parameters are summarized in Table 1. Each parameter was taken from published sources with the following rationale. The dry density and the total water content were calculated from the data of Gavriliev and Ugarov [9] for the inter-alas uplands of the Lena–Amga interfluve, i.e., for the same landscapes in which the Mundulakh, Yukechi and Churapcha boreholes are located. The unfrozen water content and the heat capacity of frozen ground are normative values for silty loams at the given water content [41]. The share of wedge ice was calculated from the geometry of the polygonal network of the Ice Complex [35]. The resulting total ice content of the section is compared with borehole counts in Section 3.1. The mean annual ground temperature is the range for the inter-alas uplands from long-term monitoring [33]. The upper boundary of the layer, z_1 = 2 m, corresponds to the typical depth of the ice-wedge tops at undisturbed sites [12,37], and the lower boundary, z_2 = 20 m, is taken as the average position of the wedge bases: the vertical extent of the wedges varies widely and exceeds 12–25 m [9], the thickness of the yedoma deposits at the Yukechi site is about 22 m [37], and the depth of penetration of the 30-year climatic signal is 16–20 m (Section 2.3). Since Q_S is linear in the layer thickness, the estimate for a particular section is rescaled proportionally. All sources are published and widely used in regional geocryology, so that the input values, the assumptions and the method itself can be independently checked.

Verification used repeated temperature logs of fourteen MPI SB RAS boreholes in the Ice Complex of Central Yakutia: boreholes 10/93 and 12/93 at the Mundulakh site and borehole 9 at the Amga site, boreholes 1 and 10 at the Yukechi site, borehole 2 at the Yunkyur site, boreholes 3 and 5 at the Churapcha site, and six boreholes on three cross-sections of the AYaM railway. The temperature profiles are given in Appendix A (Tables A1 and A2), and the calculated indicators and the diagnostic plot are presented in Section 3. The location of the boreholes is shown in Figure 2, and the lithology and cryostructure of the deposits are shown in Table 2.

The longest records are available for borehole 10/93 (undisturbed larch forest on a watershed; logging cycles on 3 September 1993 and 5 September 2024, 31 years), borehole 12/93 (a young thermokarst depression on the right-of-way of a water pipeline; cycles on 3 September 1993 and 6 September 2018, 25 years; the repeat cycle was made in borehole 12/93*, see Table A1; the 1993 profile of borehole 12/93 was also reported in [30]), borehole 10 at Yukechi (18 years) and the boreholes of the AYaM cross-sections (16 years). Borehole 9 at the Amga site (disturbed thermokarst meadow) has a short record: 27 September 2021 and 27 September 2025 (4 years).

Table 1. Design parameters of the Ice Complex deposits (from published data).

Parameter	Symbol	Value	Source
Dry density, kg/m³	ρ_d	1100 (1020–1180)	calculated from [9]
Total water content, fraction	w_{tot}	0.35 (0.25–0.45)	calculated from [9]
Unfrozen water content at −2 °C, fraction	w_w	0.05	[41]
Volumetric heat capacity of frozen ground, MJ/(m³·°C)	C_f	2.1	[41]
Volumetric fraction of wedge ice, fraction	a	0.4 (0.3–0.5)	calculated from [35]
Mean annual ground temperature, °C	T	−2 (−1.5 to −3)	[33]
Design layer (depth interval 2–20 m), m	H	18	[12,37]

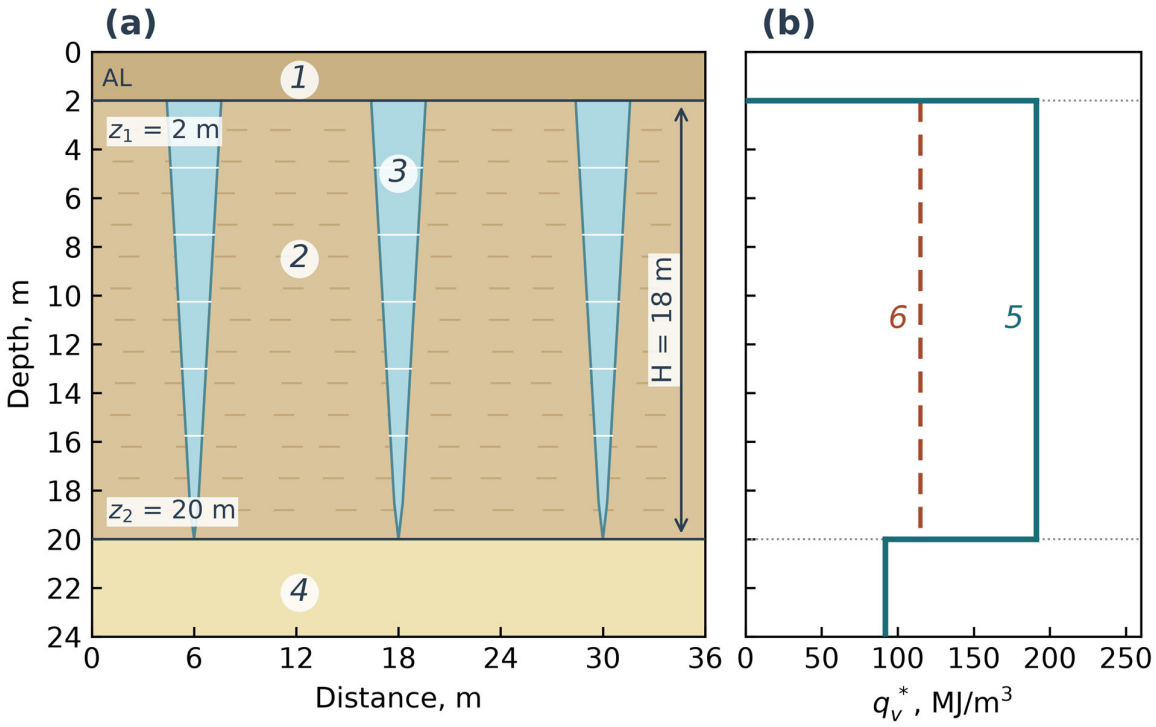

Figure 3. Scheme of a typical inter-alas section of the Ice Complex of Central Yakutia (**a**) and calculated depth distribution of the specific volumetric cold reserve at T = −2 °C (**b**): 1—active (seasonally thawed) layer, AL; 2—loess-like loams of the Ice Complex; 3—ice wedges; 4—underlying sands; 5—distribution of $q_v^*(z)$ including ice wedges (a = 0.4); 6—the same without ice wedges. z_1 and z_2 are the boundaries of the design layer of thickness H = 18 m.

Table 2. Lithology and cryostructure of the deposits at the verification boreholes (depths in meters from the ground surface).

Site, Boreholes	Landscape and Surface Condition	Lithology and Cryostructure	Ice Wedges	Ice Content *a*	Source
1. Mundulakh, boreholes 10/93 and 12/93	Inter-alas upland of the Lena–Amga interfluve east of Yakutsk. Borehole 10/93: undisturbed larch–moss–cowberry forest. Borehole 12/93: right-of-way of a water pipeline cleared in 1992, young thermokarst depression	0–1.4 (1.6) (forest) and 0–2.0 (right-of-way, 1993): active layer, silty sand and silt, w = 10–15% (forest) and 15–35% (right-of-way). 1.6–3.0: frozen silt and silty sand, w = 49–53%. 3.0–12.0 (borehole 10/93) and 2.1–14.0 (borehole 12/93): silty sand with wedge ice. 14.0–15.8: silty sand with fine-sand interlayers. 15.8–19.0: fine sand	Top at 3.0 m (forest) and 2.1 m (right-of-way); vertical extent 9–12 m	0.90 (10/93); 1.00 (12/93)	[30]
2. Yukechi, boreholes 1 and 10	Abalakh terrace 10 km east-north-east of Maya, inter-alas upland with dry and lake thermokarst depressions. Borehole 1: larch forest. Borehole 10: thermokarst meadow on former arable land, vegetation recovering	0–3.4 (3.7): silty loam, below the active layer with lenticular and layered cryostructure. 3.4 (3.7)–20: fine sand with basal ice cement, locally with layered and layered-reticulate cryostructure, fluid on thawing. Regionally, the Ice Complex is composed of silty and sandy loams with silty-sand interlayers	Top at 2.0–2.5 m; width at the top 1.5–3 m; polygons 4–6 m across	0.55 (0.5–0.6)	[12,37]; MPI SB RAS data

3. Churapcha, boreholes 3 and 5	Lena–Amga interfluve 4 km south-west of Churapcha, natural surface on both sides of the embankment of the R-504 Kolyma road. Borehole 3: ice-rich meadow with hummock-and-hollow microrelief. Borehole 5: ice-rich forest with hummock-and-hollow microrelief	Borehole 3: 0–0.2: soil and vegetation layer. 0.2–1.8: silty loam of the active layer. 1.8–10.0: ice. Borehole 5: 0–0.2: soil and vegetation layer. 0.2–2.4: loam of the active layer. 2.4–3.3: frozen loam. 3.3–10.0: ice-rich ground with a volumetric ice content of 0.6	Polygonal wedge ice; width at the top 2–5 m; polygons 5–8 m across; total volumetric ice content of the site 0.8–1.0	0.9 (0.8–1.0) for borehole 3; 0.6 (0.5–0.7) for borehole 5	MPI SB RAS data
4. Amga, borehole 9	Left bank of the Amga River near Chapchylgan, Abalakh-level terrace. Forb meadow with pronounced thermokarst relief and actively developing bylars (hummock-and-hollow microrelief), no lake; background site of the land-rehabilitation experiment on disturbed arable land	Loams and sandy loams of the Ice Complex with large ice wedges. Soil layer: frozen brown loam with grass roots. Ice Complex: frozen gray sandy loam with scattered gravel and lenticular cryostructure, containing ice wedges with vertical banding. Underlain by alluvial sands of mixed grain size with gravel and pebbles (massive cryostructure, vertical and horizontal ice lenses) and by fractured siltstones with ice-filled fractures. Active layer 2.2–2.8 m. Volumetric ice content of the deposits is elevated, about 0.5	Top at 2.2–2.5 m; vertical extent up to 15–16 m	0.50 (0.4–0.6)	[38]
5. Yunkyur, borehole 2	Lena valley terrace 5–7 km north-west of Olekminsk. Undisturbed mixed spruce–birch forest; the adjacent abandoned arable land (borehole 1) is affected by thermokarst	0–0.9: silty loam. 0.9–3.0: sandy loam with plant remains, massive cryostructure. 3.0–4.9: loam with plant remains, massive cryostructure. 4.9–7.2: wedge ice. 7.2–8.0: brown loam, massive cryostructure. Seasonal thaw depth 1.7 m; ground temperature at 8 m −1.5 °C	Top at 4.9 m (forest) and 2.0 m (abandoned arable land); width at the top 1.2–3 m; polygons 4–5 m across	0.7 (0.6–0.8)	[39]; MPI SB RAS data
6. AYaM railway, KP 693.2, 693.4 and 717.5 (boreholes B-11, B-12, B-15, B-17, B-38/09, B-39/09)	Tommot–Nizhny Bestyakh Section 80–130 km south of Yakutsk. Larch–moss–cowberry forest on east-facing slopes (KP 693.2, 693.4) and on the west-facing slope of an inter-alas upland (KP 717.5); boreholes in the forest and on the right-of-way	KP 693.2: active layer 0.7–0.8 m, soft-plastic clayey silt, w = 30–31%; frozen clayey silt, w = 39–73%; massive ice up to 6.5 m thick from 1.7–3.5 m, underlain by 2 m of very icy soil. KP 693.4: active layer 0.8–0.9 m, clayey silt, w = 24–29%; frozen silt, w = 27–132%; massive ice and icy soil 2.3–3.5 m thick from 1.2–2.1 m. KP 717.5: active layer 0.8–0.95 m, clayey silt, w = 23–24%; frozen clayey silt, w = 32–116%; ground ice from 2.3 m, more than 6 m thick	Top at 1.2–3.5 m; vertical extent 2.3 to more than 6.5 m; volumetric ice content of the ice and icy-soil layers 0.52–0.95	0.8 (693.2); 0.6 (693.4); 0.8 (717.5)	[40,45,46]

Note: w is the gravimetric moisture content. The ice content a is the total volumetric ice content of the design layer adopted in the verification calculations (Section 3.2); the range used in the Monte Carlo analysis is given in parentheses.

The lithology and cryostructure of the deposits at the verification boreholes are summarized in Table 2 from published descriptions of the sites and from the drilling logs of MPI SB RAS. At all sites, the boreholes penetrate the typical section of the Ice Complex: silty loams, sandy loams and silty sands of the active layer and of the upper frozen

horizon, underlain by ice-rich deposits with ice wedges whose tops lie at 1.2–3.5 m under natural forest and at 2.0–4.9 m where the protective layer is thicker. At the Mundulakh site, the active layer (1.4–1.6 m in the forest and 2.0 m on the pipeline right-of-way in 1993) consists of silty sands and silts; the underlying frozen silts have a gravimetric moisture content of 49–53% down to 3 m, and wedge ice occurs between 3 and 12 m [30]. At the Yukechi site, silty loams to a depth of 3.4 m are underlain by fine sands with ice cement to 20 m. The ice wedges are 1.5–3 m wide at the top, and the total volumetric ice content is 0.5–0.6 (MPI SB RAS data). At the Churapcha site, boreholes 3 and 5 are located on the natural surface on the north-western and south-eastern sides of the embankment of the R-504 Kolyma road, both with hummock-and-hollow microrelief. The polygonal wedge ice of the site is 2–5 m wide at the top with polygons 5–8 m across, and the total volumetric ice content of the deposits is 0.8–1.0 (MPI SB RAS data). According to the geocryological cross-section of the road, borehole 3 penetrates the silty loam of the active layer and, from a depth of about 1.8 m to the bottom of the borehole at 10 m, ice; borehole 5 penetrates loam of the active layer to about 2.4 m, frozen loam to about 3.3 m and, below, ice-rich ground with a volumetric ice content of 0.6. Accordingly, a = 0.9 (0.8–1.0) was adopted in the calculations for borehole 3 and a = 0.6 (0.5–0.7) for the 3–10 m layer of borehole 5. At the Amga site, the terrace is composed of loams and sandy loams of the Ice Complex with large ice wedges whose tops lie at 2.2–2.5 m and whose vertical extent reaches 15–16 m, the active layer is 2.2–2.8 m thick, and the volumetric ice content of the deposits is elevated, about 0.5 [38]. At the Yunkyur site, loams and sandy loams with plant remains overlie wedge ice at 4.9–7.2 m [39]. On the AYaM cross-sections, ice-rich clayey silts with massive ground ice from 1.2–3.5 m, 2.3 to more than 6.5 m thick, occur beneath the forest and the right-of-way [40,45,46]. The salinity of the deposits was not determined, and they are treated as non-saline (Section 4.2).

2.5. Processing of Repeated Borehole Temperature Logs

The temperature profiles were interpolated onto a 0.25 m grid, and the cold reserve was computed by (1)–(3) from the permafrost table (determined by the zero isotherm) to the bottom of the borehole. Ground parameters were taken from Table 1 without fitting. Their uncertainty was estimated by the Monte Carlo method (3000 realizations with uniform variation of the parameters within the ranges of Table 1 and of the site-specific ice content, together with random errors of the temperature measurements, the seasonal residual and the position of the permafrost table): the tables give medians and Monte Carlo intervals (10th and 90th percentiles), and for key conclusions the share of realizations in which they hold is reported, consistent with the probabilistic interpretation of stability [20]. The phase contribution of the layer removed from the frozen stratum as the permafrost table descended was accounted for by a boundary term:

$$q_r = \frac{Q_S(t_1) - Q_S(t_2)}{t_2 - t_1} + \frac{\int q_v^*(z) \cdot dz}{t_2 - t_1}, \; z \in [z_{top,1}, z_{top,2}] \quad (7)$$

where $z_{top,1}$ and $z_{top,2}$ are the positions of the permafrost table in the first and second cycles, m. The sensitivity of the estimate to an error of ±0.1 m in the permafrost table position is 0.5, 1.2 and 5.1 MJ/(m²·yr) for intervals of 31, 25 and 4 years, respectively. Therefore, intervals between cycles of at least 10 years are recommended.

The relationship between surface settlement Δs, the apparent displacement of the permafrost table and the thawed thickness H is

$$\Delta s = a \cdot H, \; d_2 - d_1 = (1 - a) \cdot H, \; H = (d_2 - d_1) + \Delta s \quad (8)$$

where d_1 and d_2 are the depths of the permafrost table below the surface in the measurement cycles, m; Δs and H are also expressed in m.

The design layer of the verification calculations is bounded above by the deeper of the two positions of the permafrost table and below by a depth of 10 m, which is the bottom of most boreholes (for the Yukechi boreholes logged to 20 m, the same limit was adopted for comparability), 8 m for borehole 2 at Yunkyur and 7 m for boreholes B-11 and B-15, where the lower part of the section was not logged in both cycles. The verification estimates (Section 3.2) therefore refer to the upper part of the design layer of Table 1 and not to the full 2–20 m stratum. This truncation is conservative. The cold reserve of the truncated layer (1.5–2.4 GJ/m² for the layers 7–8 m thick) is by construction smaller than that of the full layer (3.4 GJ/m² for the typical section), whereas the interannual change in heat content is concentrated in the upper meters of the section, so that the load q_r is underestimated only slightly. The index I_E of the truncated layer is thus biased low, i.e., toward the safe side, and the values obtained are lower bounds for the full ice-rich stratum. Since the lower boundary is set in the same way for all boreholes, the comparison between sites is not affected. The magnitude of the effect is quantified for borehole 10/93 in Section 3.2.

For use in engineering practice, the assessment is performed in the following sequence.

(1) The design layer $[z_1, z_2]$ is assigned: z_1 is the depth of the ice-wedge tops or the design depth of the foundation base, and z_2 is the base of the ice-rich horizon or the depth of zero annual amplitude.
(2) The ground parameters (ρ_d, w_{tot}, $w_w(T)$, C_f) and the ice content $a(z)$ are taken from site-investigation data or, in their absence, from regional tables such as Table 1.
(3) The cold reserve Q_S is computed by Equations (1)–(3) from the temperature profile of the first logging cycle.
(4) The load q_r is determined by Equation (4) with the boundary term (7) and the settlement correction (8) from a repeated logging cycle. Where only one profile is available, q_r is specified as a scenario for typical surface conditions (Section 3.1) or from the regional warming trend.
(5) The index I_E and the time t_Q are computed by Equations (5) and (6), and the stability class is assigned using the boundaries I_E = 1, 3 and 10.
(6) The time t_Q is compared with the design service life of the structure. Sites with $I_E < 3$ are assigned to priority monitoring and protective measures, and sites with $I_E \geq 10$ to routine monitoring at intervals of 10–15 years (Section 4.3).

The procedure uses only the data of standard site investigations and the existing observation network. A worked example for the AYaM railway right-of-way is given in Section 4.3.

3. Results

3.1. Cold Reserve and Typical Heat Loads of the Ice Complex of Central Yakutia

According to Equations (1) and (2), the specific volumetric cold reserve of the host sediment is $q_v = 2.1 \cdot 2 + 0.335 \cdot 1100 \cdot 0.30 \approx 115$ MJ/m³, that of wedge ice is about 305 MJ/m³, and the section-weighted value at $a = 0.4$ is $q_v^* \approx 191$ MJ/m³ (Figure 3b). The corresponding volumetric ice content of the section (0.62) agrees with the range of 50–80% [9] and with borehole counts on the inter-alas uplands that yielded no less than 62–64% ice [36] (p. 43). As the temperature decreases from −1 to −6 °C, the specific cold reserve increases by less than 10% (Figure 4). Equation (3) with H = 18 m gives $Q_S \approx 3.4$ GJ/m². Varying the parameters within the observed limits (w_{tot} = 0.25–0.45, a = 0.3–0.5) yields a range of 2.6–4.1 GJ/m². This value is equivalent to only about three annual radiation balances of the ground surface [13], and the stability of the stratum is entirely determined by the smallness of the net flux q_r compared with the gross heat-exchange fluxes.

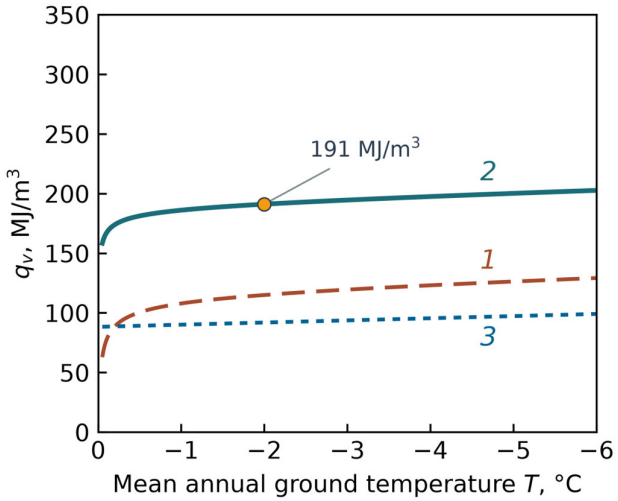

Figure 4. Specific volumetric cold reserve q_v versus mean annual ground temperature: 1—loess-like loam of the Ice Complex (w_{tot} = 0.35, without ice wedges); 2—Ice Complex deposits including ice wedges (a = 0.4); 3—frozen sand with w_{tot} = 0.18. The dot shows the calculated value q_v^* ≈ 191 MJ/m^3 at T = −2 °C.

Estimates of the index I_E and the time t_Q for typical surface conditions are given in Table 3 and Figure 5. For undisturbed forest, the load was estimated from the rate of increase in the heat content of the layer of annual heat turnover under ground warming of 0.02–0.05 °C/yr [33]: q_r ≈ 1 MJ/(m^2·yr). For disturbed surfaces and wetted depressions, the load was calculated as a scenario from the observed lowering rates of the top of ice-rich horizons of 0.03–0.16 m/yr [9] and from surface subsidence at the Yukechi site [12]. For forming lakes, it was derived from typical talik formation rates of 0.5–1.0 m/yr.

Table 3. Energy stability of the Ice Complex deposits under typical surface conditions (base case: Q_S = 3.4 GJ/m^2).

Surface Condition	q_r, MJ/(m^2·yr)	t_Q, Years	I_E	Stability Class
I. Natural conditions: undisturbed inter-alas forest	≈1	≈3400	>100	stable
II. Disturbed conditions without ponding: initial bylar, bylar and iyo stages (thaw 0.03–0.16 m/yr)	6–30	110–570	4–19	conditionally stable
III. Disturbed conditions with ponding: dyuyodya stage	30–60	60–110	2–4	weakly stable
IV. Floors of forming thermokarst lakes (thaw 0.5–1.0 m/yr)	95–190	18–36	0.6–1.2	unstable

Note: thaw rates refer to the lowering of the permafrost table. Yakut terms for successive thermokarst landforms follow [36] (pp. 12–13): initial bylar—slightly lowered surface deformed by isolated subsidence funnels and troughs; bylar—the troughs have merged into a characteristic hummocky surface; iyo—a weakly expressed hollow among the hummocky surface; dyuyodya—a depression with more or less sharply expressed sides and a hummocky floor; tympy—the first alas stage, in which the ground ice beneath the floor has melted out.

The thresholds of the scale are justified as follows. At I_E < 1, the total heat input over the normative period exceeds the cold reserve (t_Q < τ_0), and the design layer thaws within the forecast horizon. The boundary I_E = 3 acts as a safety factor: the combined uncertainty of Q_S and q_r reaches 30–50% (Monte Carlo intervals in Table 4), and a threefold margin preserves the conclusion t_Q > τ_0 even under an unfavorable combination of errors. The boundary I_E = 10 identifies states with an order-of-magnitude margin: a threefold increase in load, comparable to moving to the next row of Table 3, does not take a site out of the

conditionally stable domain. Verification (Table 4) confirms the resolving power of the scale: natural landscapes have I_E = 38–205, and disturbed sites 1.4–11.7.

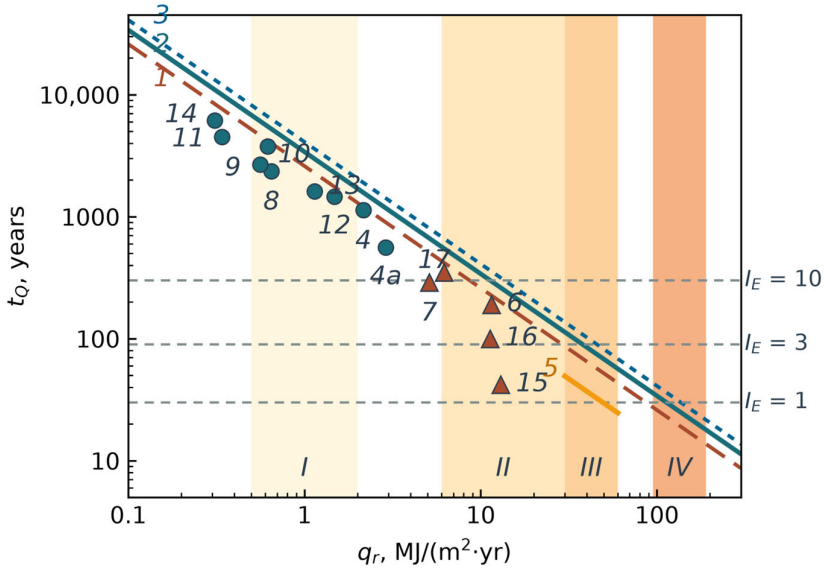

Figure 5. Characteristic exhaustion time of the cold reserve t_Q versus mean annual net heat load q_r: 1–3—Equation (6) with cold reserve Q_S, GJ/m²: 1—2.6; 2—3.4; 3—4.1. Bands I–IV show the ranges of q_r for typical surface conditions (see Table 3); horizontal dashed lines are the boundaries of stability classes by the index I_E at τ_0 = 30 years. Lines 1–3 refer to the 2–20 m design layer of the typical section (Table 1), whereas the borehole points refer to the layers of Table 4 bounded by the borehole depth (7–10 m); their t_Q are therefore lower bounds, and the points lie below the lines. Circles—boreholes under natural conditions: 4, 4a—borehole 10/93 (Mundulakh) with layer-by-layer and area-averaged ice content, respectively; 8—borehole 1 (Yukechi); 9—borehole 2 (Yunkyur); 10—borehole 3 and 11—borehole 5 (Churapcha); 12–14—forest boreholes of the AYaM railway (B-12, B-17 and B-39/09). Triangles—boreholes under disturbed conditions: 6—boreholes 12/93 and 12/93* (water pipeline right-of-way) corrected for surface settlement by Equations (7) and (8); 7—borehole 9 (Amga, thermokarst meadow); 15–17—AYaM railway right-of-way (boreholes B-11, B-15 and B-38/09; integral estimates by Equation (7)). Line 5—scenario estimate for borehole 9 under renewed ponding with the load of band III. Monte Carlo intervals of all estimates are given in Table 4; borehole 10 (Yukechi) has a negative load and therefore cannot be plotted on the logarithmic axis; its values are given in Table 4.

The classification of surface conditions in Table 3 is ordered not by the type of disturbance but by the thermokarst stage and the degree of surface wetting, in accordance with the genetic sequence of alas landforms [36] (pp. 12–15): band III is assigned to the ponded dyuyodya stage, and band IV to the floors of forming lakes, since the tympy stage already corresponds to ice that has melted out beneath the depression floor [36] (p. 13). The controlling factor is wetting: the immediate cause of degradation in depressions is the emergence and development of alas lakes [36] (p. 124), and beneath shallow water bodies thaw proceeds 1.5–2 times faster than on dry polygonal landforms [47]. The type of disturbance has a weaker effect: removal of the tree layer changes the reduced maximum ground temperature at depths of 2–10 m by only 0.3–0.6 °C, whereas a transition to a water-body floor changes it by 4–5 °C [36] (p. 98).

Frozen sand (ρ_d = 1550 kg/m³, w_{tot} = 0.18) at −2 °C has $q_v \approx$ 90 MJ/m³, half that of the Ice Complex deposits, and under equal load the exhaustion times differ by more than a factor

of two. During degradation, the temperature of ice-rich ground stabilizes near 0 °C, whereas Q_S decreases monotonically and retains its diagnostic value.

3.2. Verification Against Borehole Data

For borehole 10/93 (forest), the load was q_r = 2.2 (Monte Carlo interval 1.7–3.2) MJ/(m²·yr) with I_E = 38 (25–48), indicating a stable frozen state (point 4 in Figure 5). The high values reflect the thick ice wedge penetrated by the borehole: the specific cold reserve by the log is 290 MJ/m³ against 193 MJ/m³ for the area-averaged ice content a = 0.4. With a = 0.4, the same profiles give q_r = 2.9 MJ/(m²·yr), I_E = 19 and t_Q ≈ 560 years (point 4a). The class does not change, and the twofold difference in time reflects the real difference in the energy capacity of a wedge and of the host sediment rather than an error of the criterion, so an estimate must state to which element of the polygonal network it refers. For the area-averaged variant, the estimate was extended to the full 2–20 m layer by extrapolating the difference between the two temperature profiles below 10 m with the half-space solution, in which the temperature change at depth z is proportional to $\mathrm{erfc}[z/(2(\kappa\Delta t)^{1/2})]$, at the thermal diffusivity adopted in Section 2.3. The 10–20 m layer adds 0.6–0.7 MJ/(m²·yr) to the load, giving q_r ≈ 3.5 MJ/(m²·yr), Q_S ≈ 3.5 GJ/m², I_E ≈ 33 and t_Q ≈ 1000 years. The cold reserve of the 2–20 m layer derived from the borehole thus practically coincides with the base estimate of 3.4 GJ/m² for the typical section (Section 3.1).

For borehole 12/93 (depression), the change in the cold reserve of the 2.86–10 m layer is small (2.22 versus 2.20 GJ/m²). However, over 25 years the permafrost table descended by 0.51 m, and the boundary term (7) gives 6.9 (5.1–9.7) MJ/(m²·yr). With the observed settlement of young depressions (0.5–1.0 m over the period), the total load corrected by Equation (8) reaches q_r = 11.5 (8.5–14.6) MJ/(m²·yr), with I_E = 6.4 (5.0–8.7) and t_Q ≈ 190 (150–260) years (point 6 in Figure 5). Neglecting the boundary term and settlement would underestimate the load by a factor of about 19. The diagnosis agrees with the warming of the ground at 10 m depth from −1.9 to −1.0 °C.

For borehole 9 (disturbed meadow, 4 years), the total load was 5.1 MJ/(m²·yr), of which 2.2 is due to the increase in heat content and 2.9 to the boundary term. The index is I_E = 9.7 and t_Q ≈ 290 years (point 7). Because of the short record, the Monte Carlo interval is wide (from −6 to +18 MJ/(m²·yr)), but the positive sign of the load is retained in 74% of realizations. The residual cold reserve of the 2.85–10 m layer is 1.47 GJ/m², and the estimate is preliminary. According to the scenario calculation by Equation (6), if the site were ponded (band III of Table 3, q_r = 30–60 MJ/(m²·yr)), the index would drop to 1.6–0.8 and the exhaustion time to 25–49 years (Figure 5, line 5): the main risk is posed by wetting rather than by the current state.

Among the Mundulakh and Amga boreholes, the load of disturbed sites exceeds the background forest load by a factor of 2.3 (borehole 9, 2.85–10 m layer: 5.1 versus 2.2 for the 1.60–10 m layer of borehole 10/93) and 5.2 (borehole 12/93 with settlement correction), and the sequence of indices 38 → 9.7 → 6.4 correctly ranks the sites by the severity of thermokarst. The background load of 2–4 MJ/(m²·yr) agrees in order of magnitude with the scenario estimate in Table 3 based on regional trends of 0.02–0.05 °C/yr [33]. The borehole-based estimate is naturally higher than the averaged trend.

Table 4. Results of verification of the energy criterion against fourteen boreholes with repeated temperature logs from the MPI SB RAS monitoring network (Monte Carlo intervals, 10th–90th percentiles, in parentheses).

Site, Borehole (Surface Condition)	Logging Cycles	Design Layer, m	Ice Content of the Layer *a*, Fraction	$Q_S(t_2)$, GJ/m²	Load q_r, MJ/(m²·yr)	Index I_E	Time t_Q, Years	Stability Class
Main sample: Mundulakh, Amga, Yukechi, Yunkyur and Churapcha sites (Central Yakutia)								
Mundulakh, borehole 10/93 (undisturbed inter-alas forest)	1993–2024 (31 yr)	1.60–10	0.90	2.44 (2.38–2.48)	2.2 (1.7–3.2)	38 (25–48)	≈1130 (760–1430)	stable
Mundulakh, boreholes 12/93 and 12/93* (water pipeline right-of-way, active thermokarst)	1993–2018 (25 yr)	2.86–10	1.00	2.20 (2.15–2.22)	11.5 (8.5–14.6) [1]	6.4 (5.0–8.7)	≈190 (150–260)	conditionally stable
Amga, borehole 9 (disturbed thermokarst meadow with bylars)	2021–2025 (4 yr)	2.85–10	0.50	1.47 (1.30–1.61)	5.1 (−6 to +18)	9.7 (2.5–24.5)	≈290 (75–740); 25–49 under renewed ponding	conditionally stable; weakly stable to unstable under ponding
Yukechi, borehole 1 (inter-alas forest)	2016–2025 (9 yr)	3–10	0.55 (0.5–0.6)	1.53 (1.42–1.63)	0.7 (−0.1 to +1.5)	≈80 (33–250) [3]	≈2400 (1000–7500) [3]	stable
Yukechi, borehole 10 (thermokarst meadow, vegetation recovery)	1993–2011 (18 yr)	3–10	0.55 (0.5–0.6)	1.55 (1.44–1.65)	−0.7 (−0.9 to −0.5)	–	–	stable, accumulation of cold reserve
Yunkyur, borehole 2 (forest)	2019–2025 (6 yr)	2–8	0.7 (0.6–0.8)	1.50 (1.39–1.60)	0.6 (0.0 to +1.1)	≈90 (44–280) [3]	≈2700 (1300–8400) [3]	stable
Churapcha, borehole 3 (ice-rich meadow)	2019–2026 (7 yr)	2–10	0.9 (0.8–1.0)	2.34 (2.20–2.46)	0.6 (+0.3 to +1.0)	≈130 (81–260)	≈3800 (2400–7800)	stable
Churapcha, borehole 5 (ice-rich forest)	2019–2026 (7 yr)	3–10	0.6 (0.5–0.7)	1.65 (1.49–1.76)	0.3 (0.0 to +0.7)	≈150 (80–520) [3]	≈4500 (2400–16,000) [3]	stable
Additional sample: AYaM railway monitoring cross-sections								
KP 693.2, borehole B-12 (forest)	2009–2025 (16 yr)	2–10	0.8 (0.7–0.9)	2.16 (2.01–2.28)	1.5 (1.3–1.8)	49 (39–60)	≈1500 (1200–1800)	stable
KP 693.4, borehole B-17 (forest)	2009–2025 (16 yr)	2–10	0.6 (0.5–0.7)	1.85 (1.68–1.99)	1.1 (1.0–1.4)	54 (43–66)	≈1600 (1300–2000)	stable
KP 717.5, borehole B-39/09 (forest)	2009–2025 (16 yr)	3–10	0.8 (0.7–0.9)	1.90 (1.78–2.01)	0.31 (0.19–0.43)	205 (150–330)	≈6100 (4300–9900)	stable
KP 693.2, borehole B-11 (right-of-way)	2009–2025 (16 yr)	5–7	0.8 (0.7–0.9)	0.54 (0.51–0.58)	13.0 (10.0–16.5) [2]	1.4 (1.1–1.8) [4]	≈40 (33–54) [4]	weakly stable
KP 693.4, borehole B-15 (right-of-way)	2009–2025 (16 yr)	2–7	0.6 (0.5–0.7)	1.15 (1.04–1.24)	11.3 (9.2–13.7) [2]	3.4 (2.7–4.2) [4]	≈100 (82–125) [4]	conditionally stable
KP 717.5, borehole B-38/09 (right-of-way)	2009–2025 (16 yr)	2–10	0.8 (0.7–0.9)	2.16 (2.02–2.28)	6.2 (4.6–7.8)[2]	11.7 (9.3–15.5)	≈350 (280–470)	stable (near the class boundary)

[1] Corrected for surface settlement by Equation (8). [2] Integral load with the boundary term (7); diagnostic estimates for the frozen layer for boreholes B-11, B-15 and B-38/09: loads 0.27 (0.23–0.32), 1.0 (0.7–1.3) and 0.95 (0.76–1.17) MJ/(m²·yr); indices 67 (56–80), 38 (27–53) and 76 (59–97); times ≈2000 (1700–2400), ≈1150 (820–1600) and ≈2300 (1800–2900) years. [3] From realizations with a positive load; their share is 85%, 91% and 92% for boreholes 1, 2 and 5, respectively; for borehole 3, all realizations are positive. [4] Lower-bound estimate: the residual cold reserve is characterized by the part of the section available in both cycles (5–7 and 2–7 m). * The repeat logging cycle of 2018 was made in borehole 12/93*, which was drilled in 2008, 100 m from the original borehole 12/93 (Table A1).

Boreholes 1 (Yukechi), 2 (Yunkyur), 3 and 5 (Churapcha), with intervals of 6–9 years, complement the sample of natural conditions: the loads were 0.3–0.7 MJ/(m²·yr) with indices no lower than 30 (points 8–11). For borehole 10 at Yukechi (an overgrowing meadow), the load over 1993–2011 was negative, q_r = −0.7 (−0.9 to −0.5) MJ/(m²·yr): the cold reserve accumulated as vegetation recovered, and the criterion captures not only degradation but also recovery. The range of natural loads over the six boreholes was −0.7 to 2.2 MJ/(m²·yr).

Six boreholes on three cross-sections of the AYaM railway (KP 693.2, 693.4 and 717.5) [40] compare forest and right-of-way pairwise using temperature profiles of 11–12 September 2009 and 3 September 2025 (16 years). In the forests (boreholes B-12, B-17 and B-39/09), the loads were 0.3–1.5 MJ/(m²·yr) with indices of 49–205 (points 12–14), within the natural range for Central Yakutia. On the right-of-way (boreholes B-11, B-15 and B-38/09), the integral loads by Equation (7) were 6.2–13.0 MJ/(m²·yr) with indices from 11.7 down to 1.4 (points 15–17, band II). The forest-to-right-of-way contrast reaches a factor of 9–20. Surface settlement on the right-of-way was not measured, so the estimates are lower bounds. After the initial thaw, degradation manifests itself almost exclusively as lowering of the permafrost table: the diagnostic loads without the boundary term were only 0.27–1.0 MJ/(m²·yr) (footnote 2 of Table 4), which confirms that the complete form (7) is required.

The indicators in Table 4 clearly separate the sample. Nine boreholes in natural and recovering landscapes, with loads from −0.7 to 2.2 MJ/(m²·yr) and residual reserves of 1.50–2.44 GJ/m², are stable: the eight with a positive load have I_E = 38–205 and t_Q ≈ 1130–6100 years, and at borehole 10 (Yukechi) the cold reserve was accumulating. The five disturbed sites form a sequence of decreasing index: borehole B-38/09 remains at the lower boundary of the stable class (I_E = 11.7, t_Q ≈ 350 years), boreholes 9, 12/93 and B-15 fall into the conditionally stable class (I_E = 9.7, 6.4 and 3.4), and borehole B-11 into the weakly stable class (I_E = 1.4, t_Q ≈ 40 years). The times of 40–350 years are many times shorter than those of natural sites. There are no unstable states in the sample: a transition to this class is predicted only by the ponding scenario (Figure 5, line 5).

4. Discussion

4.1. Comparison with Existing Approaches

The proposed criterion is not an alternative to temperature monitoring but complements it with an energy measure that remains sensitive near 0 °C. It differs from ordinal scales and zoning maps [21–24] in being metric, in explicitly accounting for the acting heat load, and in combining temperature and ice content into a single quantity Q_s instead of a point-based score. Ice content is not lost from the risk assessment: it determines both the phase capacity and the potential settlement $\Delta s = a \cdot H$ upon exhaustion of the reserve.

In existing approaches, the external thermal impact is accounted for by climatic indices [17], temperature-trend response indicators [18,19], probabilistic convolution [20] or a balance scheme of winter heat losses and summer heat gains [48]. The energy criterion differs in that the load and the capacity are expressed in the same units (J/m²), the load is determined from actual borehole data, and the result takes the form of a safety margin, by analogy with engineering design. The probabilistic interpretation is retained as the share of Monte Carlo realizations.

The closest in purpose is the geothermal stability criterion G_k, based on the ratio of the actual ground temperature to the limiting temperature for the formation of non-merging permafrost [16]. G_k diagnoses proximity to the threshold of restructuring of the thermal regime of the layer of annual heat turnover and is convenient for rapid zoning from temperature data, whereas the energy criterion quantifies the load, rate and time of

degradation after it has begun. The two criteria thus address successive stages of the same process.

In the international context, this work brings to the applied level the enthalpy-based interpretation of permafrost degradation [15] and the method of enthalpy processing of repeated temperature profiles [29]. The comparison with interior Alaska requires a clarification of the source and comparability of the values. The loads of 4–12 MJ/(m²·yr) quoted in Section 2.3 are the mean heat fluxes into permafrost of 0.13–0.39 W/m² reported by Nicolsky and Romanovsky [29] for the Old Man and Birch Lake sites, converted by us to MJ/(m²·yr) (1 W/m² = 31.5 MJ/(m²·yr)). These fluxes were obtained by the same enthalpy method as Equation (4): the change in the sum of the sensible and latent heat content of the ground between temperature profiles measured 8–28 years apart, integrated from a depth of 2 m to the depth of 60 m at which the temperature change vanishes, and divided by the time interval [29]. The method is thus identical, but the integration depth differs. The loads of the Yakutian boreholes refer to the 2–10 m (3–10 m) layer, and the heat absorbed below 10 m is not counted, so they are lower bounds. Rescaling of the forest borehole 10/93 with the area-averaged ice content to the 2–20 m layer raises the load from 2.9 to about 3.5 MJ/(m²·yr) (Section 3.2), which brings it close to the lower limit of the Alaskan range. The 28-year mean at both Alaskan sites, 0.15 W/m² or 4.7 MJ/(m²·yr) [29], is only 1.3 times higher.

The remaining difference has a physical explanation in the thermal state of the ground and in the climate. The Alaskan sites are located in the discontinuous permafrost zone with a mean annual ground temperature of about −1 °C [29]. The climate there is milder and snowier: the mean annual air temperature at Fairbanks is −2.1 °C and the annual precipitation is 296 mm (1991–2020 normals) [49], against −8.0 °C and about 235 mm at Yakutsk (1981–2020) with a late-winter snow depth of only 25–40 cm [30]. In warm permafrost the unfrozen-water curve is steep, and a unit of warming consumes several times more heat than in cold permafrost. For the Fairbanks silt curve used in [29], warming from −1.0 to −0.5 °C increases the unfrozen water content by about 2% of dry mass, which at ρ_d = 1100 kg/m³ corresponds to about 8 MJ/m³ of latent heat, whereas the same step from −3.0 to −2.5 °C requires about 1.2 MJ/m³. The sensible component, about 1 MJ/m³, is the same in both cases (estimated by the authors with C_f from Table 1). The same climatic forcing therefore produces an approximately fourfold larger enthalpy change, i.e., a larger q_r, in the warm permafrost of interior Alaska than in the colder permafrost of Central Yakutia, where the latent part of the load is realized mainly at the permafrost table. This is consistent with the verification results: the loads of the Yakutian forest boreholes are small, although the ground at 10 m depth warmed by 0.1–0.7 °C per decade (Tables A1 and A2), whereas the loads of the disturbed Yakutian sites, 5–13 MJ/(m²·yr), where thaw at the permafrost table dominates, overlap the natural Alaskan range.

In terms of the present thermal balance, the natural sites of Central Yakutia and the permafrost observatories of Alaska and northern Canada show the same sign and a similar magnitude of change. Permafrost temperatures near the depth of zero annual amplitude increased on average by 0.39 ± 0.15 °C in the continuous and by 0.20 ± 0.10 °C in the discontinuous permafrost zone between 2007 and 2016 [50]. In northern Canada and Alaska, warm permafrost (warmer than −2 °C) is warming at less than 0.3 °C per decade, whereas the cold permafrost of the Arctic is warming at up to about 1 °C per decade [51]. The forest boreholes of Central Yakutia warmed at 10 m depth by 0.1–0.7 °C per decade (Tables A1 and A2), that is, at rates typical of the North American permafrost regions. The energy equivalent of these rates differs, however, with the thermal state of the ground. In cold permafrost (−5 to −10 °C) with negligible unfrozen water, a warming of 0.5–1 °C per decade of a 20 m layer with $C_f \approx 2$ MJ/(m³·°C) corresponds to a purely sensible load of 2–4 MJ/(m²·yr), which consumes about 1% of the cold reserve per decade.

Such ground remains stable by the criterion ($I_E > 10$) despite the high warming rate. In the warm permafrost of interior Alaska and the southern discontinuous zone of Canada, the same forcing yields 4–12 MJ/(m²·yr) [29], mainly through the latent component and at an almost constant temperature. The natural sites of Central Yakutia (−0.7 to 2.2 MJ/(m²·yr) for the 2–10 m layer and up to 3.5 MJ/(m²·yr) for the 2–20 m layer) occupy the lower part of this range, and the disturbed sites (5–13 MJ/(m²·yr)) coincide with the natural Alaskan range. In all three regions, the net flux into the permafrost is of the order of 0.1–0.4 W/m², i.e., about 1% of the annual radiation balance of the surface or less, which is why permafrost temperature alone is a weak indicator of the loss of the cold reserve and why the energy criterion is transferable to these regions (Section 4.2).

Direct comparison with numerical modeling (Table 5) shows that the linear estimate t_Q is 1.4–1.7 times shorter than the modeled time, which agrees with its conservative nature and justifies the interval [t_Q; t_{SI}] as a rapid forecast. Transient simulations of a gravel road on continuous permafrost show a similar two-phase behavior of degradation, an initial phase of slow gradual thaw followed by a sharp acceleration once a critical ground warming is exceeded, and the transition can occur within the service life of the structure of about 30 years [52]. The index I_E and the time t_Q provide a simple way to locate a site relative to this transition from repeated borehole data.

Table 5. Comparison of the criterion with numerical modeling of the degradation of a homogeneous frozen soil column [29]; μ is the constant heat flux prescribed at the ground surface in the model.

Indicator	μ = 0.2 W/m² (Natural Surface)	μ = 1 W/m² (Disturbed Surface)
Heat load q_r, MJ/(m²·yr)	6.3	31.6
Thickness of the forming talik in the model, m	10	20
Cold reserve of the layer Q_S by (1)–(3), GJ/m²	1.15	2.30
Index I_E by (5)	6.1	2.4
Stability class on the proposed scale	conditionally stable	weakly stable
Exhaustion time t_Q by (6), years	182	73
Talik formation time in the numerical model, years	300	100
Ratio of the modeled time to t_Q	1.7	1.4

4.2. Limits of Applicability and Data Requirements

The limits of applicability are determined by the assumptions: one-dimensional heat transfer, neglect of convection and moisture migration, and linearity of extrapolation (6). For sites with intense seepage, near water bodies and on slopes, the estimate requires corrections or numerical modeling. The conservatism of (6) preserves the role of the criterion as a lower-bound estimate of time. The load q_r is non-stationary and averages fluctuations of opposite sign (for example, the negative load at borehole 10 at Yukechi). The index should be recalculated as logging cycles accumulate, as a moving characteristic of monitoring.

The verification sample, with intervals between cycles from 4 to 31 years, makes it possible to compare the informativeness of different intervals. The load error consists of two parts: an additive part related to the seasonal residual and the accuracy of thermometry, whose contribution to q_r decreases in inverse proportion to the interval, and a multiplicative part related to the uncertainty of ice content and water content, which is proportional to the load itself and is not removed by lengthening the record. Short intervals therefore perform poorly under weak loads: with a 4-year interval (borehole 9), the Monte Carlo interval of the load was −6 to +18 MJ/(m²·yr) and the sign was retained in only 74% of realizations. With 6–9-year intervals (boreholes 1, 2, 3 and 5), the sign was stable in 85–100% of realizations, but the width of the load intervals (0.7–1.6 MJ/(m²·yr)) was comparable to the loads themselves. With 16-year intervals (AYaM forests), the width

decreased to 0.24–0.5 MJ/(m²·yr). The downside of long intervals is the loss of timeliness and averaging over non-stationarity: the 18-year interval of borehole 10 (Yukechi) combines stages of degradation and vegetation recovery, and the internal dynamics of the process cannot be reconstructed from two cycles. A reasonable compromise for natural landscapes with loads of 1–2 MJ/(m²·yr) appears to be 10–15 years. Intervals shorter than 5 years are justified only as a preliminary estimate at rapidly degrading sites, where the load is several times the background, whereas intervals longer than 20–30 years give reliable mean values but characterize the past rather than the current state.

The parameterization and verification of the criterion are deliberately based on single temperature measurements at the end of the warm season: such single profiles are what engineering site investigations and a considerable part of observation-network boreholes provide, and the criterion has been shown to work with the most accessible type of data. The price of this accessibility is the seasonal residual included in the uncertainty budget (±0.2 °C in the 2–6 m layer) and the requirement of close calendar dates of the cycles. Where data-logger records are available, monthly mean or, better, annual mean temperatures are preferable: annual averaging removes the seasonal cycle, eliminates the requirement for matching dates and substantially narrows the load intervals, especially for short intervals between cycles. Equations (1)–(8) remain unchanged.

The transition to areal estimates requires averaging the cold reserve and the load separately over landscape elements, rather than averaging the ready indices. The share of wedge ice is estimated from the geometry of the polygonal network: with wedge width b and network spacing D, the volumetric fraction is $a \approx 2b/D - (b/D)^2$. For b = 2–3 m and D = 11–14 m [35], this gives a = 0.27–0.47, consistent with Table 1. An independent areal estimate of the load is provided by repeated terrestrial laser scanning [53]: a value of 21 MJ/(m²·yr) characterizes areas of active thermokarst and serves as an upper bound for the inter-alas uplands. About six boreholes are needed to characterize a landscape element with an error of about 15%.

Other limitations relate to the input data: the accuracy of determining the permafrost table, the matching of cycles to close dates, and the representativeness of the parameters in Table 1. The convective component during infiltration of summer precipitation can add 1.0–2.7 MJ/(m²·yr) and, under wet conditions, makes the estimates by Equation (4) lower bounds. All verification values are either direct calculations from the temperature profiles in Tables A1 and A2 or scenario estimates explicitly labeled as such.

A further limitation concerns the salinity of the deposits. Equation (1) is written for non-saline ground, for which the temperature of the onset of thawing is close to 0 °C and the unfrozen water content at −2 °C is small (Table 1). In saline frozen ground, the freezing point is depressed, the curve $w_w(T)$ is shifted toward lower temperatures, and part of the pore moisture remains unfrozen at the temperatures typical of the Ice Complex. For such ground, the cold reserve must be computed relative to the actual temperature of the onset of thawing T_{bf}, which is determined from the salinity and the composition of the pore solution [41,42], with the measured curve $w_w(T)$. Both the sensible and the latent components then decrease, and the index I_E of saline deposits at the same temperature and ice content is lower than that of non-saline deposits. The formulation (1) allows this through $w_w(T)$ and the limit T_{bf}, but the parameterization in Table 1 and the verification refer to the Ice Complex of the inter-alas uplands, which is formed by continental sediments and is treated as non-saline. The salinity of the deposits was not determined in the verification boreholes. For weakly saline silty loams, the depression of T_{bf} is a few tenths of a degree, and the resulting decrease in Q_S lies within the uncertainty of the ice content (Section 3.1). Application of the criterion to the saline marine and lagoonal deposits of the Arctic coastal lowlands requires site-specific determination of T_{bf} and $w_w(T)$.

https://doi.org/10.3390/geosciences16120486

The applicability of the criterion to other permafrost regions follows from its structure. The cold reserve and the load are computed everywhere from the same inputs, i.e., temperature profiles, ice content, water content and the unfrozen-water curve, and only the parameterization (Table 1) is regional. In the continuous zone of cold permafrost (northern Yakutia, the North Slope of Alaska, the Canadian Arctic Archipelago), the reserve is large, and the loads are mostly sensible, so that I_E is high and the criterion mainly ranks disturbed sites and tracks the consumption of the reserve before thaw begins. In the discontinuous zone with warm permafrost (interior Alaska, the Mackenzie Valley, the southern margin of the permafrost zone in Siberia), where temperature monitoring is least informative, the criterion is most useful, because the loss of the cold reserve proceeds at an almost constant temperature. The same applies to the Qinghai–Tibet Plateau, where nearly 40% of the permafrost is warmer than −0.5 °C and about 60% of the existing infrastructure is projected to fall within the high-hazard zone of permafrost degradation by 2090 [54]. Here the unfrozen-water curve must be determined carefully, since it controls both Q_S and q_r (Section 4.1). In coastal settlements, the criterion describes only the thermal part of the hazard: thermal abrasion and thermal erosion of the coast, lateral heat exchange with the sea and the salinity of the deposits are not included in the one-dimensional balance (1)–(8), and the thermal estimate of t_Q should be regarded as optimistic for the coastal zone. Long-term monitoring in the western Russian Arctic, where ground temperatures at 10–12 m depth have risen by 0.03–0.06 °C/yr and the permafrost table has lowered by up to 8 m in the discontinuous zone, distinguishes stable, unstable and actively degrading permafrost [55]; the energy criterion offers a metric basis for such staging. In mountain permafrost, the criterion is applicable to flat sites with conductive heat transfer but not to coarse blocky deposits with convective cooling. Boreholes in the European mountains warmed at 10 m depth by 0.2–0.6 °C per decade on regional average in 2013–2022 and by more than 1 °C per decade at some sites, whereas ice-rich ground near 0 °C warmed least because of latent heat effects [56,57]; such sites are precisely where the cold reserve, rather than the temperature, should be tracked. In all cases, a regional analog of Table 1 and at least two logging cycles are required.

4.3. Implications for Geohazard Mitigation and Adaptation

From the standpoint of geohazard mitigation and adaptation, the criterion converts site-investigation and monitoring data into two quantities that can be used directly in decision-making. First, t_Q is a time-based measure of the thaw hazard that can be compared with the design service life of a structure. On the AYaM railway right-of-way, borehole B-11 falls into the weakly stable class with $t_Q \approx 40$ years (Table 4), i.e., the cold reserve of the upper permafrost there may be exhausted within a period comparable to the service life of the embankment, whereas the neighboring forest (borehole B-12) retains a reserve of about 1500 years. Sites with $I_E < 3$ are therefore natural candidates for priority monitoring and protective measures, while sites with $I_E \geq 10$ can be monitored at the routine interval of 10–15 years recommended above.

Second, because I_E is inversely proportional to q_r (Equation (5)), any measure that reduces the heat load, such as drainage of the right-of-way, preservation or restoration of the vegetation and organic cover, or engineering cooling of the foundation (convection embankments, thermosyphons) [2], raises the index in proportion to the reduction in load, and its effect can be verified with the same repeated borehole logs. The results indicate where such measures matter most. Surface wetting is the controlling factor of degradation (Section 3.1), and the scenario for borehole 9 shows that renewed ponding would lower the index from 9.7 to 1.6–0.8 (Figure 5, line 5). Preventing water ponding along linear infrastructure therefore appears to be the key measure for the Ice Complex. Conversely, the negative load at borehole 10 (Yukechi) shows that vegetation recovery on a disturbed

site restores the cold reserve, so the criterion can also document the effect of adaptation and land rehabilitation measures.

Finally, since the cold reserve and the heat load are additive quantities, the criterion can be extended to maps by combining permafrost–landscape maps, which provide Q_S through ice content and ground temperature, with load estimates for each landscape type and disturbance class (Table 3). Such maps would provide a quantitative basis for thaw-hazard zoning along existing and planned transport corridors in ice-rich permafrost.

5. Conclusions

1. The concept of the cold reserve of a frozen stratum, its enthalpy deficit relative to the onset of thawing, is introduced, and an energy-based criterion of thermal stability is built on it. The criterion consists of the dimensionless index I_E, the ratio of the cold reserve to the total heat input over the 30-year normative period, and the characteristic exhaustion time t_Q. Equations (1)–(3) account for unfrozen water and, separately, for ice wedges and are computed from standard site-investigation data. Four stability classes with boundaries I_E = 1, 3 and 10 are distinguished. The linear estimate t_Q is conservative, and the upper bound is given by the Stefan approximation.
2. The heat load q_r is determined by enthalpy processing of repeated borehole temperature logs using Equations (4), (7) and (8), with account for the displacement of the permafrost table and surface settlement, from the existing observation network and single end-of-warm-season measurements. For natural landscapes, intervals of 10–15 years between cycles are recommended. Intervals shorter than 5 years give only the sign and order of magnitude of the load, and intervals longer than 20–30 years characterize the past rather than the current state. Monthly and annual mean temperatures, where available, narrow the load intervals without changing the governing equations.
3. For a typical inter-alas section of the Ice Complex of Central Yakutia, the cold reserve of the 2–20 m layer is 2.6–4.1 GJ/m^2, with a specific volumetric value of about 191 MJ/m^3. Verification against fourteen boreholes with intervals from 4 to 31 years showed that the loads of natural landscapes were −0.7 to 2.2 MJ/(m^2·yr) with indices of 38–205, and those of disturbed thermokarst-affected sites, including the AYaM railway right-of-way, were 5.1–13.0 MJ/(m^2·yr) with indices from 11.7 down to 1.4. The sequence of indices correctly ranked the sites by the severity of degradation; a negative load captured the accumulation of the cold reserve during vegetation recovery, and surface wetting was identified as the controlling factor of degradation. The natural loads of Central Yakutia lie at the lower end of, and the disturbed loads within, the range of 4–12 MJ/(m^2·yr) reported for interior Alaska.
4. The criterion remains sensitive near 0 °C and is applicable to ranking sites, setting priorities for monitoring and mitigation of thaw-related geohazards, rapid assessment of degradation time relative to the service life of structures, and evaluation of protective and rehabilitation measures, including the development of regulations on permafrost protection [23]. Its transfer to other permafrost regions requires only a regional parameterization of the cold reserve and, for saline and coastal deposits, the actual temperature of the onset of thawing and the unfrozen-water curve.

Author Contributions: Conceptualization, A.Z. and M.Z.; methodology, A.Z., M.Z. and Z.W.; software, A.Z.; validation, T.W. and G.L.; formal analysis, A.Z.; investigation, A.F., P.K. and V.L.; resources, M.Z. and A.F.; data curation, P.K., A.F. and V.L.; writing (original draft preparation), A.Z.; writing (review and editing), M.Z., Z.W., A.F., T.W., P.K., G.L. and V.L.; visualization, A.Z. and V.L.; supervision, M.Z. and Z.W.; project administration, A.Z. All authors have read and agreed to the published version of the manuscript.

Funding: These studies were supported by a grant from the Ministry of Science and Higher Education of the Russian Federation (agreement No. 075-15-2024-554 of 24 April 2024) and the Fundamental Scientific Research Program in the Russian Federation (projects No. 126020216324-9 and No. 126020516688-9).

Institutional Review Board Statement: Not applicable.

Informed Consent Statement: Not applicable.

Data Availability Statement: The borehole temperature profiles used for verification are provided in Appendix A (Tables A1 and A2). Other data supporting the findings of this study are available from the corresponding author upon reasonable request.

Conflicts of Interest: The authors declare no conflicts of interest.

Abbreviations

The following abbreviations are used in this manuscript:

AL	active layer
AYaM	Amur–Yakutsk Mainline railway
KP	kilometer post
MPI SB RAS	Melnikov Permafrost Institute, Siberian Branch of the Russian Academy of Sciences

Appendix A

Table A1. Temperature profiles of the verification boreholes at the Mundulakh, Amga, Yukechi, Yunkyur and Churapcha sites in Central Yakutia, °C (MPI SB RAS data; the 1993 profile of borehole 12/93 was also reported in [30]).

Depth, m	Mundulakh, Borehole 10/93		Mundulakh, Boreholes 12/93 and 12/93*		Amga, Borehole 9		Yukechi, Borehole 1		Yukechi, Borehole 10		Yunkyur, Borehole 2		Churapcha, Borehole 3		Churapcha, Borehole 5	
	3 September 1993	5 September 2024	3 September 1993	6 September 2018	27 September 2021	27 September 2025	20 September 2016	3 September 2025	19 August 1993	8 September 2011	15 September 2019	15 September 2025	16 September 2019	19 September 2026	16 September 2019	19 September 2026
0	–	–	–	–	–	–	–	–	–	–	4.59	6.24	–	–	–	–
1	0.2	1.2	6.3	8.1	4.78	5.44	3.2	6.3	9.6	5.7	3.13	3.26	3.12	1.44	4.19	3.85
2	−1.0	−0.8	0.6	1.9	1.59	1.97	0.1	0.6	1.1	−0.2	−1.21	−1.21	−1.33	−0.98	0.76	0.03
3	−1.8	−1.3	−1.1	−0.3	−0.45	−0.34	−0.6	−0.5	−0.8	−1.2	−1.47	−1.22	−1.58	−1.38	−1.53	−1.41
4	−2.3	−1.7	−1.4	–	−0.56	−0.49	−0.7	−0.6	–	–	–	–	−1.9	−1.69	−2.04	−1.93
5	−2.7	−1.9	−1.7	−0.4	−0.66	−0.59	−0.9	−0.7	−1.2	−1.4	–	–	−2.01	−1.86	−2.40	−2.22
6	–	–	–	–	–	–	–	–	–	–	−1.49	−1.31	−2.18	−1.96	−2.52	−2.43
7	−3.9	−3.6	−1.8	–	–	–	–	–	−0.8	−1.5	–	–	−2.29	−2.00	−2.71	−2.55
7.5	–	–	–	–	−0.79	−0.73	–	–	–	–	–	–	–	–	–	–
8	–	–	–	–	–	–	–	–	–	–	−1.54	−1.28	−2.29	−2.00	−2.70	−2.58
9	–	–	–	–	–	–	–	–	–	–	–	–	−2.35	−2.01	−2.71	−2.60
10	−2.8	−2.0	−1.90	−1.0	−0.96	−0.90	−1.2	−1.1	−0.9	−1.3	–	–	−2.36	−2.00	−2.73	−2.57

Note: a dash means that no measurement was made at this depth. * Borehole 12/93* was drilled in 2008, 100 m from the original borehole 12/93; the profile of 6 September 2018 was measured in this borehole.

Table A2. Temperature profiles of the boreholes on the AYaM railway monitoring cross-sections, °C (MPI SB RAS data; cross-sections described in [40]).

Depth, m	Borehole B-12 (KP 693.2, Forest)		Borehole B-17 (KP 693.4, Forest)		Borehole B-39/09 (KP 717.5, Forest)		Borehole B-11 (KP 693.2, Right-of-Way)		Borehole B-15 (KP 693.4, Right-of-Way)		Borehole B-38/09 (KP 717.5, Right-of-Way)	
	11 September 2009	3 September 2025	11 September 2009	3 September 2025	12 September 2009	3 September 2025	11 September 2009	3 September 2025	11 September 2009	3 September 2025	12 September 2009	3 September 2025
1	−0.4	0.7	−0.6	1.4	−0.3	2.6	1.0	9.0	−0.2	9.0	0.0	5.4
2	−1.4	−0.7	−1.4	−0.7	−1.1	–	−2.1	0.2	−1.2	−0.65	−1.2	−0.8
3	–	–	–	–	−1.5	−1.3	–	–	–	–	–	–
5	−2.2	−0.9	−2.2	–	−1.8	−1.6	−2.8	−2.0	−1.9	−0.9	−1.8	−1.0
7	−2.3	−1.0	−2.5	−1.8	−2.0	−1.66	−3.1	−2.0	−2.1	−0.95	−2.0	−1.1
10	−2.2	−1.1	−2.3	−1.5	−2.0	−1.63	−3.2	–	−2.2	–	−2.0	−1.3

Note: a dash means that no measurement was made at this depth.

References

1. Hjort, J.; Karjalainen, O.; Aalto, J.; Westermann, S.; Romanovsky, V.E.; Nelson, F.E.; Etzelmüller, B.; Luoto, M. Degrading permafrost puts Arctic infrastructure at risk by mid-century. *Nat. Commun.* **2018**, *9*, 5147. https://doi.org/10.1038/s41467-018-07557-4.
2. Hjort, J.; Streletskiy, D.; Doré, G.; Wu, Q.; Bjella, K.; Luoto, M. Impacts of permafrost degradation on infrastructure. *Nat. Rev. Earth Environ.* **2022**, *3*, 24–38. https://doi.org/10.1038/s43017-021-00247-8.
3. Streletskiy, D.A.; Clemens, S.; Lanckman, J.-P.; Shiklomanov, N.I. The costs of Arctic infrastructure damages due to permafrost degradation. *Environ. Res. Lett.* **2023**, *18*, 015006. https://doi.org/10.1088/1748-9326/acab18.
4. Streletskiy, D.A.; Suter, L.J.; Shiklomanov, N.I.; Porfiriev, B.N.; Eliseev, D.O. Assessment of climate change impacts on buildings, structures and infrastructure in the Russian regions on permafrost. *Environ. Res. Lett.* **2019**, *14*, 025003. https://doi.org/10.1088/1748-9326/aaf5e6.
5. Czerniawska, J.; Chlachula, J. Climate-change induced permafrost degradation in Yakutia, East Siberia. *Arctic* **2020**, *73*, 509–528. https://doi.org/10.14430/arctic71674.
6. Takakura, H. Limits of pastoral adaptation to permafrost regions caused by climate change among the Sakha people in the middle basin of Lena River. *Polar Sci.* **2016**, *10*, 395–403. https://doi.org/10.1016/j.polar.2016.04.003.
7. Takakura, H.; Fujioka, Y.; Ignatyeva, V.; Tanaka, T.; Vinokurova, N.; Grigorev, S.; Boyakova, S. Differences in local perceptions about climate and environmental changes among residents in a small community in Eastern Siberia. *Polar Sci.* **2021**, *27*, 100556. https://doi.org/10.1016/j.polar.2020.100556.
8. Doloisio, N.; Vanderlinden, J.-P. The perception of permafrost thaw in the Sakha Republic (Russia): Narratives, culture and risk in the face of climate change. *Polar Sci.* **2020**, *26*, 100589. https://doi.org/10.1016/j.polar.2020.100589.
9. Gavriliev, P.P.; Ugarov, I.S. Response of the Ice Complex deposits of Central Yakutia to climate warming. *Earth's Cryosphere* **2009**, *13*, 24–30. (In Russian)
10. Nitzbon, J.; Westermann, S.; Langer, M.; Martin, L.C.P.; Strauss, J.; Laboor, S.; Boike, J. Fast response of cold ice-rich permafrost in northeast Siberia to a warming climate. *Nat. Commun.* **2020**, *11*, 2201. https://doi.org/10.1038/s41467-020-15725-8.
11. Streletskiy, D.A.; Maslakov, A.; Grosse, G.; Shiklomanov, N.I.; Farquharson, L.; Zwieback, S.; Iwahana, G.; Bartsch, A.; Liu, L.; Strozzi, T.; et al. Thawing permafrost is subsiding in the Northern Hemisphere: Review and perspectives. *Environ. Res. Lett.* **2025**, *20*, 013006. https://doi.org/10.1088/1748-9326/ada2ff.
12. Fedorov, A.N.; Konstantinov, P.Y. Observations of surface dynamics with thermokarst initiation, Yukechi site, Central Yakutia. In *Proceedings of the 8th International Conference on Permafrost, Zürich, Switzerland, 21–25 July 2003*; Swets & Zeitlinger: Lisse, The Netherlands, 2003; pp. 239–243.
13. Pavlov, A.V. *Monitoring of the Cryolithozone*; Academic Publishing House "Geo": Novosibirsk, Russia, 2008. (In Russian)
14. Ershov, E.D. *General Geocryology*; Moscow University Press: Moscow, Russia, 2002. (In Russian)
15. Nitzbon, J.; Krinner, G.; Schneider von Deimling, T.; Werner, M.; Langer, M. First quantification of the permafrost heat sink in the Earth's climate system. *Geophys. Res. Lett.* **2023**, *50*, e2022GL102053. https://doi.org/10.1029/2022GL102053.
16. Galkin, A.F.; Zheleznyak, M.N.; Zhirkov, A.F.; Baluta, V.I. Geothermal criterion for assessing the stability of frozen soils in seasonally active permafrost. *Arct. Subarct. Nat. Resour.* **2024**, *29*, 543–552. https://doi.org/10.31242/2618-9712-2024-29-4-543-552. (In Russian)
17. Kaverin, D.A.; Lapteva, E.M.; Shchanov, V.M.; Pastukhov, A.V.; Sharaya, L.S.; Shary, P.A. Climatic geoinformation analysis of the cryolithozone in the northeast of European Russia. *Earth's Cryosphere* **2019**, *23*, 68–78. https://doi.org/10.21782/KZ1560-7496-2019-4(68-78). (In Russian)
18. Pavlov, A.V.; Malkova, G.V. Small-scale mapping of trends of the contemporary ground temperature changes in the Russian North. *Earth's Cryosphere* **2009**, *13*, 32–39. (In Russian)
19. Malkova, G.V.; Pavlov, A.V.; Skachkov, Y.B. Assessment of permafrost stability under contemporary climatic changes. *Earth's Cryosphere* **2011**, *15*, 33–36. (In Russian)
20. Kozlov, A.N.; Parmuzin, S.Y.; Pustovoit, G.P. The probabilistic forecast for the average annual temperature of soils and their resistance to thawing and freezing. *Earth's Cryosphere* **1999**, *3*, 26–31. (In Russian)
21. Grave, N.A. Principles of assessing the sensitivity of the ground surface to technogenic impacts (case study of Yakutia). In *Nature Conservation in Yakutia*; Yakutsk Branch of the Siberian Branch of the USSR Academy of Sciences: Yakutsk, Russia, 1979; pp. 91–94. (In Russian)

22. Parmuzin, S.Y. Zoning of the north of West Siberia by the potential for thermokarst development. In *Problems of Geocryological Mapping*; Permafrost Institute of the Siberian Branch of the USSR Academy of Sciences: Yakutsk, Russia, 1986; pp. 78–85. (In Russian)
23. Kalinicheva, S.V. Assessment of the permafrost landscapes stability in Eastern Siberia: The case of Yakutia. *Vestn. North-East. Fed. Univ. Ser. Earth Sci.* **2024**, *3*, 51–59. https://doi.org/10.25587/2587-8751-2024-3-51-59. (In Russian)
24. Tumel, N.V.; Zotova, L.I. *Geoecology of the Cryolithozone*; Faculty of Geography, Lomonosov Moscow State University: Moscow, Russia, 2014. (In Russian)
25. Tumel, N.; Zotova, L. Diagnostics and mapping of geoecological situations in the permafrost zone of Russia. *Geosciences* **2019**, *9*, 353. https://doi.org/10.3390/geosciences9080353.
26. Kudryavtsev, V.A. (Ed.) *General Permafrost Science (Geocryology)*; Moscow University Press: Moscow, Russia, 1978. (In Russian)
27. Balobaev, V.T. *Geothermy of the Frozen Zone of the Lithosphere of Northern Asia*; Nauka: Novosibirsk, Russia, 1991. (In Russian)
28. Komarov, I.A. *Thermodynamics and Heat and Mass Transfer in Dispersed Frozen Soils*; Nauchnyi Mir: Moscow, Russia, 2003. (In Russian)
29. Nicolsky, D.J.; Romanovsky, V.E. Modeling long-term permafrost degradation. *J. Geophys. Res. Earth Surf.* **2018**, *123*, 1756–1771. https://doi.org/10.1029/2018JF004655.
30. Varlamov, S.; Skryabin, P.; Zhirkov, A.; Wen, Z. Monitoring the permafrost conditions along pipeline routes in Central Yakutia, Russia. *Land*. **2022**, *11*, 2331. https://doi.org/10.3390/land11122331.
31. Desyatkin, A.; Fedorov, P.; Filippov, N.; Desyatkin, R. Climate change and its influence on the active layer depth in Central Yakutia. *Land*. **2021**, *10*, 3. https://doi.org/10.3390/land10010003.
32. Fedorov, A.N.; Vasilyev, N.F.; Torgovkin, Y.I.; Shestakova, A.A.; Varlamov, S.P.; Zheleznyak, M.N.; Shepelev, V.V.; Konstantinov, P.Y.; Kalinicheva, S.S.; Basharin, N.I.; et al. Permafrost-landscape map of the Republic of Sakha (Yakutia) on a scale 1:1,500,000. *Geosciences* **2018**, *8*, 465. https://doi.org/10.3390/geosciences8120465.
33. Varlamov, S.P.; Skachkov, Y.B.; Skryabin, P.N. *Monitoring of the Ground Thermal Regime in Central Yakutia*; Melnikov Permafrost Institute SB RAS: Yakutsk, Russia, 2021; 156 p. (In Russian)
34. Skryabin, P.N.; Varlamov, S.P. Anthropogenic impacts on the thermal condition of permafrost in Central Yakutia. *IOP Conf. Ser. Earth Environ. Sci.* **2022**, *988*, 042006. https://doi.org/10.1088/1755-1315/988/4/042006.
35. Ivanov, M.S. *Cryogenic Structure of Quaternary Deposits of the Lena–Aldan Depression*; Nauka: Novosibirsk, Russia, 1984. (In Russian)
36. Soloviev, P.A. *The Cryolithozone of the Northern Part of the Lena–Amga Interfluve*; USSR Academy of Sciences Publishing House: Moscow, USSR, 1959. (In Russian)
37. Windirsch, T.; Grosse, G.; Ulrich, M.; Schirrmeister, L.; Fedorov, A.N.; Konstantinov, P.Y.; Fuchs, M.; Jongejans, L.L.; Wolter, J.; Opel, T.; et al. Organic carbon characteristics in ice-rich permafrost in alas and Yedoma deposits, central Yakutia, Siberia. *Biogeosciences* **2020**, *17*, 3797–3814. https://doi.org/10.5194/bg-17-3797-2020.
38. Sivtsev, M.A.; Zhirkov, A.F.; Baluta, V.I. Assessment of the possibility of restoration and protection of territories disturbed by thermokarst in Central Yakutia. *Earth's Cryosphere* **2026**, *30*, 29–41. Available online: https://earthcryosphere.ru/arch/2026-5/ (accessed on 19 November 2026). (In Russian)
39. Suleymanov, A.A.; Lytkin, V.M.; Vinokurova, L.I.; Grigoryev, S.A.; Fedorov, S.I.; Golomareva, V.Y.; Basharin, N.I.; Aprosimov, D.A. Rural communities of Yakutia in conditions of permafrost degradation: Key risks, social consequences, and adaptation mechanisms. *Arct. North.* **2023**, *52*, 168–195. https://doi.org/10.37482/issn2221-2698.2023.52.199.
40. Varlamov, S.P. Thermal monitoring of railway subgrade in a region of ice-rich permafrost, Yakutia, Russia. *Cold Reg. Sci. Technol.* **2018**, *155*, 184–192. https://doi.org/10.1016/j.coldregions.2018.06.016.
41. *SP 25.13330.2020*; Bases and Foundations on Permafrost Soils. Updated Edition of SNiP 2.02.04-88; Ministry of Construction of the Russian Federation: Moscow, Russia, 2020. (In Russian)
42. *GOST 25100-2020*; Soils. Classification. Standartinform: Moscow, Russia, 2020. (In Russian)
43. Shur, Y.L. *The Upper Horizon of Permafrost and Thermokarst*; Nauka: Novosibirsk, Russia, 1988. (In Russian)
44. World Meteorological Organization. *WMO Guidelines on the Calculation of Climate Normals*; WMO-No. 1203; WMO: Geneva, Switzerland, 2017.
45. Varlamov, S.P. Engineering-geocryological monitoring on a section of the Ice Complex deposits along the Tommot–Yakutsk railway. *Uspekhi Sovrem. Estestvozn.* **2015**, *1*, 410–414. Available online: https://natural-sciences.ru/article/view?id=34903 (accessed on 14 November 2026). (In Russian)

46. Varlamov, S.P.; Skryabin, P.N. Thermal state of grounds along the railway route in the Ice Complex area. *Mezhdunar. Zh. Prikl. Fundam. Issled.* **2015**, *10*, 517–522. Available online: https://applied-research.ru/article/view?id=7534 (accessed on 14 November 2026). (In Russian)
47. Bosikov, N.P. Wetness variability and dynamics of thermokarst processes in Central Yakutia. In *Proceedings of the 7th International Conference on Permafrost, Yellowknife, Canada, 1998*; Collection Nordicana No. 55; Centre d'études Nordiques, Université Laval: Québec, Canada, 1998; pp. 71–74.
48. Marakhtanov, V.P. Thermomechanical thawing of ground (idea and calculation method). *Earth's Cryosphere* **2006**, *10*, 59–67. (In Russian)
49. NOAA National Centers for Environmental Information. U.S. Climate Normals 1991–2020: Fairbanks International Airport, AK (USW00026411). Available online: https://www.ncei.noaa.gov/access/us-climate-normals/ (accessed on 14 November 2026).
50. Biskaborn, B.K.; Smith, S.L.; Noetzli, J.; Matthes, H.; Vieira, G.; Streletskiy, D.A.; Schoeneich, P.; Romanovsky, V.E.; Lewkowicz, A.G.; Abramov, A.; et al. Permafrost is warming at a global scale. *Nat. Commun.* **2019**, *10*, 264. https://doi.org/10.1038/s41467-018-08240-4.
51. Smith, S.L.; O'Neill, H.B.; Isaksen, K.; Noetzli, J.; Romanovsky, V.E. The changing thermal state of permafrost. *Nat. Rev. Earth Environ.* **2022**, *3*, 10–23. https://doi.org/10.1038/s43017-021-00240-1.
52. Schneider von Deimling, T.; Lee, H.; Ingeman-Nielsen, T.; Westermann, S.; Romanovsky, V.; Lamoureux, S.; Walker, D.A.; Chadburn, S.; Trochim, E.; Cai, L.; et al. Consequences of permafrost degradation for Arctic infrastructure: Bridging the model gap between regional and engineering scales. *Cryosphere* **2021**, *15*, 2451–2471. https://doi.org/10.5194/tc-15-2451-2021.
53. Lytkin, V.M.; Basharin, N.I.; Zhirkov, A.F.; Kirillin, A.R.; Sivtsev, M.A. Application of a terrestrial laser scanner to study the annual and interannual variability of thermokarst in Central Yakutia. *Curr. Probl. Remote Sens. Earth Space* **2023**, *20*, 130–139. https://doi.org/10.21046/2070-7401-2023-20-5-130-139. (In Russian)
54. Ran, Y.; Cheng, G.; Dong, Y.; Hjort, J.; Lovecraft, A.L.; Kang, S.; Tan, M.; Li, X. Permafrost degradation increases risk and large future costs of infrastructure on the Third Pole. *Commun. Earth Environ.* **2022**, *3*, 238. https://doi.org/10.1038/s43247-022-00568-6.
55. Vasiliev, A.A.; Drozdov, D.S.; Gravis, A.G.; Malkova, G.V.; Nyland, K.E.; Streletskiy, D.A. Permafrost degradation in the Western Russian Arctic. *Environ. Res. Lett.* **2020**, *15*, 045001. https://doi.org/10.1088/1748-9326/ab6f12.
56. Etzelmüller, B.; Guglielmin, M.; Hauck, C.; Hilbich, C.; Hoelzle, M.; Isaksen, K.; Noetzli, J.; Oliva, M.; Ramos, M. Twenty years of European mountain permafrost dynamics: The PACE legacy. *Environ. Res. Lett.* **2020**, *15*, 104070. https://doi.org/10.1088/1748-9326/abae9d.
57. Noetzli, J.; Isaksen, K.; Barnett, J.; Christiansen, H.H.; Delaloye, R.; Etzelmüller, B.; Farinotti, D.; Gallemann, T.; Guglielmin, M.; Hauck, C.; et al. Enhanced warming of European mountain permafrost in the early 21st century. *Nat. Commun.* **2024**, *15*, 10508. https://doi.org/10.1038/s41467-024-54831-9.

Disclaimer/Publisher's Note: The statements, opinions and data contained in all publications are solely those of the individual author(s) and contributor(s) and not of MDPI and/or the editor(s). MDPI and/or the editor(s) disclaim responsibility for any injury to people or property resulting from any ideas, methods, instructions or products referred to in the content.